Î²2 Adrenergic-Neurotrophin Feedforward Loop Promotes Pancreatic Cancer

HHS Public Access

Author manuscript

Cancer Cell. Author manuscript; available in PMC 2019 January 08.

Published in final edited form as:

Cancer Cell. 2018 January 08; 33(1): 75–90.e7. doi:10.1016/j.ccell.2017.11.007.

β2 adrenergic-neurotrophin feed-forward loop promotes pancreatic cancer

Bernhard W. Renz[1,2,14], **Ryota Takahashi**[2,14], **Takayuki Tanaka**[2], **Marina Macchini**[2,3], **Yoku Hayakawa**[2,4], **Zahra Dantes**[5], **H. Carlo Maurer**[2], **Xiaowei Chen**[2,†], **Zhengyu Jiang**[2], **C. Benedikt Westphalen**[2,6], **Matthias Ilmer**[1], **Giovanni Valenti**[2], **Sarajo K. Mohanta**[7], **Andreas J. R. Habenicht**[7], **Moritz Middelhoff**[2], **Timothy Chu**[2], **Karan Nagar**[2], **Yagnesh Tailor**[2], **Riccardo Casadei**[8], **Mariacristina Di Marco**[9], **Axel Kleespies**[1], **Richard A. Friedman**[10], **Helen Remotti**[11], **Maximilian Reichert**[5], **Daniel L. Worthley**[2,12], **Jens Neumann**[13], **Jens Werner**[1], **Alina C. Iuga**[11], **Kenneth P. Olive**[2,11], and **Timothy C. Wang**[2,15,*]

[1]Department of General, Visceral and Transplantation Surgery, Hospital of the University of Munich, D-81377, Munich, Germany

[2]Department of Digestive and Liver Diseases and Herbert Irving Comprehensive Cancer Center, Columbia University Medical Center, New York, NY 10032, USA

[3]Department of Oncology, IRCCS San Raffaele Scientific Institute, 20132 Milan, Italy

[4]Department of Gastroenterology, Graduate School of Medicine, The University of Tokyo, Tokyo, 113-8655, Japan

[5]Department of Medicine II, Klinikum Rechts der Isar, Technische Universität München, D-81675 Munich, Germany

[6]Department of Internal Medicine III, Hospital of the University of Munich, D-81377, Munich, Germany

[7]Institute for Cardiovascular Prevention, University of Munich, D-80336, Munich, Germany

[8]Department of Internal Medicine and Surgery (DIMEC), Alma Mater Studiorum, University of Bologna, Sant'Orsola-Malpighi Hospital, 40138 Bologna Italy

[9]Department of Experimental, Diagnostic and Speciality Medicine, University of Bologna, Sant'Orsola-Malpighi Hospital, 40138 Bologna, Italy

[*]**Corresponding author:** Timothy C. Wang, M.D., Division of Digestive and Liver Diseases, Columbia University Medical Center, 1130 St. Nicholas Avenue, New York, NY 10032 USA, Phone: (212) 851 4581, Fax: (212) 851 4590, tcw21@columbia.edu.

[14]These authors contributed equally

[15]Lead Contact

[†]Deceased

AUTHOR CONTRIBUTIONS

Conceptualization, B.W.R., R.T., and T.C.W.; Methodology, B.W.R., C.B.W. and M.R.; Formal analysis, R.A.F.; Investigation, B.W.R., R.T., T.T., M.M., Y.H., Z.D., H.C.M., X.C., Z.J., C.B.W., M.I., G.V., S.K.M., M.M., T.C., K.N., Y.T., H.R., D.L.W., J.N., and A.C.I.; Resources, A.J.R.H., R.H., R.C., M.D.M., A.K., H.R., and J.W.; Writing-original Draft, B.W.R., R.T., T.C.W.; Writing-Review and Editing, B.W.R., R.T. and T.C.W.; Supervision, B.W.R., K.P.O. and T.C.W.

[10]Biomedical Informatics Shared Resource, Herbert Irving Comprehensive Cancer Center, and Department of Biomedical Informatics, Columbia University Medical Center, New York, NY 10032, USA

[11]Department of Pathology and Cell Biology, Columbia University Medical Center, New York, NY 10032, USA

[12]Department of Medicine, University of Adelaide, SA, 5005, Australia

[13]Department of Pathology Hospital of the University of Munich, D-81377, Munich, Germany

Summary

Catecholamines stimulate epithelial proliferation, but the role of sympathetic nerve signaling in pancreatic ductal adenocarcinoma (PDAC) is poorly understood. Catecholamines promoted ADRB2 dependent PDAC development, nerve growth factor (NGF) secretion, and pancreatic nerve density. Pancreatic *Ngf* overexpression accelerated tumor development in LSL-*Kras*$^{+/G12D}$;*Pdx1*-Cre (KC) mice. ADRB2 blockade together with gemcitabine reduced NGF expression and nerve density, and increased survival of LSL-*Kras*$^{+/G12D}$;LSL-*Trp53*$^{+/R172H}$;*Pdx1*-Cre (KPC) mice. Therapy with a Trk-inhibitor together with gemcitabine also increased survival of KPC mice. Analysis of PDAC patient cohorts revealed a correlation between BDNF expression, nerve density, and increased survival of patients on non-selective β-blockers. These findings suggest that catecholamines drive a feed-forward loop, whereby upregulation of neurotrophins increases sympathetic innervation and local norepinephrine accumulation.

Graphical abstract

Renz et al. show that norepinephrine (NE) promotes ADRB2-dependent pancreatic ductal adenocarcinoma development and secretion of neurotrophins (NT), which in turn promote tumor innervation leading to increased NE and tumor growth. Blockade of ADRB2 or NT receptors improves gemcitabine’s therapeutic effect.

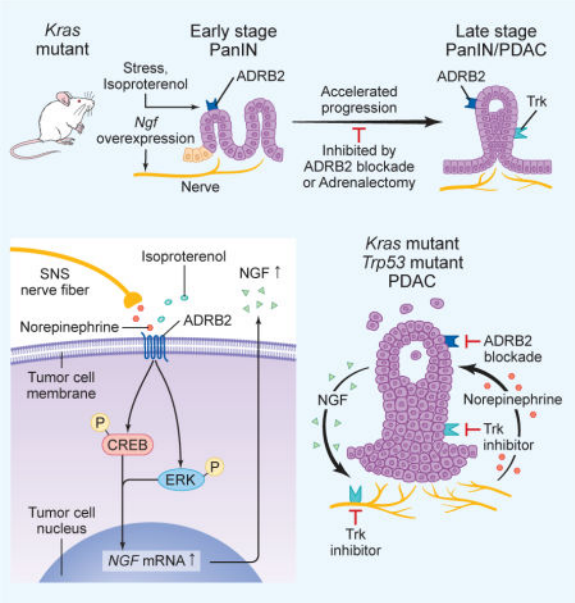

Introduction

Patients with pancreatic ductal adenocarcinoma (PDAC) have a median survival of 6 months and by 2030 PDAC is predicted to be the second leading cause of cancer-related death in the U.S. (Rahib et al., 2014). PDAC is characterized by a complex desmoplastic stroma that includes immune cells, endothelial cells, stellate cells, nerves, and matrix proteins. This heterogeneous cellular environment acts in concert to reduce tumor immunity and to provide growth factors and neurotransmitters essential for tumor growth (Apte and Wilson, 2012; Demir et al., 2015).

Mouse models expressing an endogenous oncogenic *Kras* in pancreatic exocrine lineages can reproduce human pancreatic intraepithelial neoplasia (PanIN) (Hingorani et al., 2003), but progression to PDAC requires additional factors (Guerra et al., 2007). While some of these stimulatory factors are likely provided by inflammatory leukocytes, the role of the nervous system in supporting tumor growth needs to be considered. Recent studies have shown the importance of the autonomic nervous system in tumorigenesis for prostate cancer (Magnon et al., 2013; Zahalka et al., 2017), ovarian cancer (Thaker et al., 2006), gastric cancer (Hayakawa et al., 2017; Zhao et al., 2014), and basal cell carcinoma (Peterson et al., 2015).

The pancreas is innervated by both sympathetic and parasympathetic nerves (Borden et al., 2013). In contrast to the normal pancreas, PDAC is characterized by high neural density, marked neural hypertrophy, and overexpression of norepinephrine (NE), suggesting that PDAC cells stimulate nerve growth in their local microenvironment (Ceyhan et al., 2009). Tumor cells have been shown to attract nerves, presumably by secreting neurotrophins (NT) such as NGF, BDNF, NT3, and NT4. NTs are a family of growth factors that stimulate nerve growth and mediate axonal guidance, synaptic plasticity and protection of nerves from injury, but can also act as autocrine growth factors and potentiate tumor cell invasion (Bapat

et al., 2016). In this respect, it is important to note that intra- and extra-pancreatic perineural invasion by cancer cells is present in 71%–100% of PDAC resection specimens, and associated with worse patient survival (Liebl et al., 2014).

The sympathetic nervous system (SNS) is an anatomical and functional network of nerves, the adrenal medulla and their respective neurotransmitters and receptors. Catecholamines, including epinephrine (EPI) and norepinephrine (NE), act on effector tissues through α- and β-adrenergic receptors, which are widely expressed in both normal and neoplastic tissues including PDAC cell lines (Weddle et al., 2001). Catecholamines are stress molecules, produced by the SNS and linked to PDAC growth via β-adrenergic signaling using *in vitro* (Guo et al., 2013; Zhang et al., 2010) and *in vivo* studies (Kim-Fuchs et al., 2014). It is known from epidemiologic studies that stress can promote tumor growth (Jansen et al., 2014) and that PDAC patients have the highest level of psychological stress of all investigated types of cancer (Clark et al., 2010). In addition, cancer mortality is significantly increased by high levels of psychological stress (Batty et al., 2017). On the other hand, it is suggested that β-blocker treatment of patients suffering from colorectal cancer (Jansen et al., 2014), breast cancer (Barron et al., 2011), ovarian cancer (Watkins et al., 2015), melanoma (Lemeshow et al., 2011), and PDAC (Beg et al., 2017; Udumyan et al., 2017), may lead to improved survival.

Systemic stress has been shown to accelerate growth of cancer cells grown in immunocompromised mice, including ovarian cancer (Thaker et al., 2006), prostate cancer (Hassan et al., 2013), and PDAC xenografts (Kim-Fuchs et al., 2014) and allografts (Partecke et al., 2016) models. However, the role of stress on early progression of *Kras* mutant pancreatic cells has not been addressed. The role of physiological and psychological stress drivers in PDAC led us to investigate the hypothesis that stress might biologically promote directly the growth of PDAC via β-adrenergic signaling.

Results

Chronic Neuropsychological Stress Promotes *Kras* Induced Pancreatic Carcinogenesis

To investigate the effects of systemic catecholamines on PDAC initiation, we utilized KC (LSL-*Kras*$^{+/LSL\text{-}G12D}$;*Pdx1*-Cre) mice. In this model, animals 20 weeks of age or less show few PanIN-1A lesions, with the vast majority of ducts appearing normal. By 7–10 months, more neoplastic lesions (82% of total) are observed, which are mostly low-grade (PanIN-1A and 1B) (65%), but include a substantial number of grade PanIN-2 (16%) and occasional PanIN-3 lesions (Hingorani et al., 2003).

Chronic restraint stress (CRS), which led to increased circulating systemic epinephrine levels (Figure 1A), was induced by daily repeated immobilization (Figure 1B). Pathological scoring at 20 weeks of age revealed that the area of normal pancreas in CRS mice was significantly smaller than in control mice (Figure S1A). Importantly, PDAC lesions, not observed in unstressed KC mice, were present in 38% of the KC CRS mice (Figures 1C-E).

The β2-adrenergic receptor (ADRB2) is reported to be the major mediator for chronic stress induced cancers, including PDAC (Schuller et al., 2011), and we observed a significant

upregulation of *Adrb2* mRNA in KC pancreata (Figure 1F). In addition, ADRB2 protein was expressed strongly in areas of dysplasia compared to WT pancreata (Figures 1G and H). Treatment with the specific ADRB2 antagonist ICI 118,551 (ICI) reduced PDAC incidence compared to untreated KC animals subjected to CRS only (Figures 1C,E and I).

In contrast, treatment with isoproterenol (ISO), a broad β-adrenergic agonist, potentiated carcinogenesis, leading to a 77% incidence of PDAC (Figure 1C and Figure S1B). When KC-*Adrb2* KO mice were exposed to CRS, PDAC was detected in only 12% (Figure 1C and Figure S1C). CRS led to hypertrophy of the adrenal glands, with increased adrenal gland weight/body weight ratio (ADW/BW) (Figures S1D and S1E), while treatment with ISO lowered this ratio and reduced adrenal size, presumably due to negative feedback on adrenal catecholamine production. To confirm a role for adrenal-derived catecholamines in the acceleration of PDAC, we performed bilateral adrenalectomy (ADx) in KC mice at 6 weeks of age, and then applied the CRS model (KC CRS ADx). Tumor incidence was reduced and comparable to the ICI group (Figure 1C and Figure S1F).

Staining for ADRB2 in pancreata from KC mice revealed a cytoplasmic granular staining pattern in acinar tissue (Figure S1G) and a membranous pattern in neoplastic ducts, particularly in KC CRS mice (Figure S1H). Our interpretation of this pattern is that oncogenic *Kras* leads to an upregulation of ADRB2, which is detected in the cytoplasm of acinar cells as a granular staining pattern. Following exposure to either CRS (Figure S1H) or ISO treatment (Figure S1I), the receptor is translocated to the cellular membrane followed by aggregation in response to ligand stimulation, leading to the more intensive staining pattern seen in early PanIN lesions. The membranous expression pattern was reduced by the ADRB2 antagonist ICI (Figure S1J) and ADx (Figure S1K) and absent in the pancreas of stressed KC-*Adrb2* KO mice (Figure S1L).

Staining of pancreata for the pan-neuronal marker peripherin revealed an increased neuronal area in KC CRS mice compared to regular KC mice (Figures 1J, K and L). This stress-dependent increase in neuronal tissue was significantly inhibited by ICI treatment (Figures 1L and M). Furthermore, neuronal tissue was increased in KC mice receiving ISO in comparison to control KC mice (Figure 1L and N) and it was significantly decreased in KC CRS ADx mice compared to KC CRS mice (Figure 1L and O). Taken together, these results suggest that chronic stress and increased circulating catecholamines lead to an expansion of intrapancreatic nerves.

ADRB2 Blockade Significantly Increases Overall Survival in KPC Mice

We next utilized the LSL-*Kras*$^{+/LSL\text{-}G12D}$;LSL-*Trp53*$^{+/R172H}$;*Pdx1*-Cre (KPC) model, which develops early PanIN lesions at 7 to 9 weeks of age, advanced PanIN lesions at 13 to 15 weeks, and PDAC by 17-19 weeks (Hingorani et al., 2005). KPC tumors show a significant increase in *Adrb2* expression compared to WT pancreata (Figure 2A) and neuropathological changes similar to those described in human disease (Ceyhan et al., 2009; Stopczynski et al., 2014). Peripherin staining (Figure 2B) showed that pancreata displaying invasive PDAC had a neuronal density of 6.62±1.31 nerves/mm^2, representing a 10-fold increase in comparison to WT pancreata (0.652±0.061 nerves/mm^2) (Figure 2C). Furthermore, pancreata from mice with PDAC had a 30-fold increase in nerve area when compared to normal pancreas

(3.203±1.15% vs. 0.1058±0.0093%) (Figure 2D). Immunoreactivity for GAP-43, a protein involved in neurite formation, regeneration and plasticity (Benowitz and Routtenberg, 1997), was indeed restricted to the neural components in PDAC. We found an increase in GAP-43 immunoreactivity and >15-fold increase in *Gap43* mRNA expression in PDAC compared to WT pancreata (Figures S2A-C).

In advanced PDAC in KPC mice, we found substantial neural invasion (Figures S2D-F). We quantified intrapancreatic sympathetic nerves, marked by expression of tyrosine hydroxylase (TH) and known to secrete NE, and noted a significantly larger TH^+ area in PDAC from KPC mice compared to WT pancreata (1.245±0.191% vs. 0.123±0.055%) (Figures 2E and F).

In order to inhibit sympathetic nervous input to the tumor, we administered ICI daily along with gemcitabine (GEM) biweekly, to KPC mice with pancreatic tumors between 20-60 mm^3. Treatment with GEM ICI significantly increased overall survival (OS) of KPC animals to 31 days, compared to 18 days in control animals treated with GEM alone (Figure 2G). As shown by the tumor volume curves (Figure 2H), growth of the tumors was inhibited by co-treatment with GEM ICI compared to GEM alone. While tumor growth was reduced by ICI treatment, tumor histopathology was otherwise unchanged (Figure S2G). This suggests that adrenergic signaling, specifically through the ADRB2, is an important driver of KPC tumorigenesis.

To test the role of local sympathetic nerves, we surgically sympathectomized (ganglionectomy or Gx) the pancreas of KPC mice once tumors reached a size of 20–60 mm^3. Combined treatment of GEM Gx significantly extended OS to 36 days, in comparison to GEM only treated mice at 18 days (Figure S2H). These findings are consistent with the notion that locally delivered catecholamines contribute to the growth of established tumors.

To test whether nerve growth and catecholamine delivery is induced by adrenergic signaling itself, we quantified the percentage of peripherin positive nerves in PDAC of KPC mice treated by GEM, GEM ICI or GEM Gx. The percentage of $peripherin^+$ structures was significantly reduced in tumors of the GEM ICI and the GEM Gx groups (Figures 2I and J). Although the overall staining pattern of ADRB2 was not markedly different in the GEM ICI and GEM Gx groups (Figure S2I), we found significant upregulation of the *Adrb2* transcript in PDAC of KPC mice treated by GEM Gx (Figure S2J). Similarly, KPC cells treated with ICI showed a significant increase *Adrb2* expression, while treatment with ISO led to a significant down-regulation of *Adrb2* (Figure S2K), thereby arguing for a regulated ligand-receptor mechanism. To confirm the ADRB2 antibody specificity, brain from WT mice, as well as brain and pancreas sections from *Adrb2* KO mice, were stained (Figure S2L). Overall, the data suggests that nerve outgrowth in pancreatic carcinogenesis is at least partly dependent on ADRB2 signaling. As expected, the staining pattern for the sympathetic neurotransmitter NE did not change in PDAC of ICI treated animals. Nevertheless, an epithelial staining pattern was observed in PDAC of GEM Gx animals (Figure S2M) suggesting that upregulation of NE expression in cancer cells acts in an autocrine fashion.

Catecholamines Promote Acinar to Ductal Metaplasia and Drive Proliferation

Next, we investigated the underlying mechanisms by which adrenergic signaling stimulates PDAC development. We assessed the sphere-forming capacity of *Kras* mutant pancreas-derived acinar cells in response to adrenergic stimulation in an established 3D culture system known to mimic acinar to ductal metaplasia (ADM) (Collins et al., 2014), the proposed first step of PDAC carcinogenesis (Kopp et al., 2012). *Kras* mutant spheres were generated from LSL-*Kras*$^{+/LSL\text{-}G12D}$ pancreata by adenovirally delivered Cre recombinase (Adeno-Cre). Cultures treated with ISO formed significantly more spheres, with a trend towards a larger size, in comparison to controls (Figures 3A-C). This stimulatory effect of ISO was blocked by pretreatment with the nonselective β-receptor blocker propranolol and ICI, but not by the ADRB1-selective agent atenolol (Figure 3B and Figure S3A). This was reflected in the expression of *Adrb2* within these spheres (Figure S3B). To validate these ADRB2-mediated findings, we also used LSL-*Kras*$^{+/LSL\text{-}G12D}$;*Adrb2* KO spheres after Adeno-Cre infection and found that these cultures showed no increase in sphere number after ISO treatment (Figures 3D-F). Furthermore, *Kras* mutant spheres treated with ISO expressed higher levels of stemness-related genes such as *Oct3/4* and *Sox9* (Figure 3G).

ADRB2 is a Gs-coupled 7-transmembrane receptor known to signal through downstream phosphokinase A (PKA) and mitogen-activated protein kinase (MAPK) pathways (Lorton and Bellinger, 2015). Thus, spheres were treated with a PKA inhibitor (KT5720) and/or a MAPK/ERK kinase (MEK) inhibitor (U0126). The MEK inhibitor reduced sphere formation, even below the basal rate, whereas PKA inhibition did not (Figure 3H and Figure S3C). These experiments were also reproduced in KC-*Adrb2* KO spheres (Figure S3D). Taken together, the data suggests that PKA signaling is primarily responsible for the direct enhancement of sphere forming capacity by ISO, and argues further for the presence of additional important inputs to MEK, beyond catecholaminergic signaling.

We next developed a local, neural model for catecholamine delivery during in vitro ADM. In this Matrigel embedded model, adapted from one previously described (Ceyhan et al., 2008), murine embryonic dorsal root ganglia (DRGs) were implanted adjacent to *Kras* mutant spheres (Figure 3I). After 7 days, there were significantly more spheres in the DRG co-cultures than in controls (Figures 3J and K). Furthermore, pretreatment of these co-cultures with ICI blocked the increase in sphere number.

As the 3D culture studies showed effects of ADRB2 signaling on pre-neoplastic acinar tissue, we next tested effects of ADRB2 signaling on PDAC cells known to express ADRB1 and ADRB2, including BxPC-3, Mia PaCa-2, and Panc-1 cell lines (Zhang et al., 2010). qRT-PCR (Figure S3E) and immunofluorescence staining (Figure S3F) confirmed ADRB2 expression by human PDAC cell lines. Human PDAC cell lines stimulated with ISO showed an increase in proliferation (Figure S3G) that could be blocked by propranolol and ICI but not by atenolol. As shown in Figures 3L and M, the phosphorylated extracellular signal-regulated kinase (pERK)/ERK ratio and the phosphorylated cAMP response element binding protein (pCREB)/CREB ratio were increased after ISO and NE treatment, an effect that was blocked by ICI pretreatment. In contrast phosphorylated p38 (pp38), phosphorylated yes-associated protein (pYAP) and phosphorylated lκBα (plκBα) were

unchanged after ISO treatment. Similar results were obtained for the complementary experiments in KPC cell lines (Figures S3H and I).

Adrenergic Signaling Increases Neurotrophin Secretion and Promotes PDAC Development through Tumor-Associated Axonogenesis

Catecholamines interact directly with tumor cells, and the initial increase in systemic epinephrine led to increased nerve density in KC mice. We hypothesized that catecholamines mediate nerve-tumor interactions by inducing neurotrophins (NT) through a feedforward loop, similar to that recently described (Hayakawa et al., 2017). We assessed NT expression in KPC tumors, which were sorted for $EpCAM^+$ and $EpCAM^-$ cells. This analysis revealed that among genes encoding for various NTs/axonal guidance proteins, *Ngf* had the highest expression level. The expression of other genes encoding for NTs (*Bdnf, Ntf3* and *Ntf4*), *Gdnf* and the axonal guidance protein netrin 1 gene (*Ntn1*) were detectable, but at lower levels (Figure 4A). This was also reproduced in a murine PDAC cell line (Figure S4A). *Ngf* was also upregulated during early tumorigenesis, with moderate increases in PanIN-bearing pancreata from KC mice and larger increases in KPC tumors (Figure 4B).

To determine whether catecholamines regulate NGF secretion from PDAC cells, KPC-derived K8282 cells were stimulated with NE. Higher concentrations of NE resulted in dose-dependent increases in *Ngf* mRNA (Figure 4C). This upregulation was reversed by ICI, KT5720 or U0126 (Figure 4D). ELISA confirmed that treatment with 10 μM NE significantly increased NGF secretion, which was not reversed by atenolol but was blocked by ICI, propranolol, KT5720, and U0126, indicating a role for PKA and ERK pathways in adrenergic-dependent NGF secretion (Figure 4E and Figure S4B). Upregulation of *Ngf* mRNA was confirmed in KC spheres treated with NE, which was inhibited by ICI (Figure S4C). As expected, spheres from KC-*Adrb2* KO mice did not show upregulation of *Ngf* mRNA after stimulation with either NE or ISO (Figure S4D).

To assess the biological significance of catecholamine-induced NGF secretion, we used the DRG co-culture model and measured neurite outgrowth by confocal imaging (Figure 4F). Treatment of the PDAC cells/DRG co-culture system with ISO markedly increased the outgrowth of neurites from DRGs at 4, 6 and 10 days (Figures 4G and H). Pretreatment with ICI blocked the outgrowth of neurites almost completely at 10 days. These *in vitro* results suggest that ADRB2-dependent upregulation of NGF contributes to an increase in nerve-cancer interactions through axonogenesis. In order to rule out the possible effects of ISO or ICI on DRG cells, rather than direct effects on tumor cells, DRGs were grown in monocultures and treated with ISO and ICI as additional controls (Figure S4E).

We crossed KC mice with *Rosa26*-LSL-*Ngf*-IRES-eGFP (N) knock-in mice (Hayakawa et al., 2017), thus achieving conditional pancreatic *Ngf* overexpression in KC mice (KCN). Analysis of the KCN pancreas confirmed a significant increase in *Ngf* expression (Figure S4F). Pancreatic neuronal tissue in general, and TH^+ sympathetic neurons in particular, were increased (Figures 4I and J). Strikingly, KCN mice at 20 weeks developed prominent nerves and intrapancreatic ganglia (Figures 4K and L), along with foci of micronodular small duct and large duct intraepithelial proliferation with cytological atypia (PanIN-3) (Figures 4M and N).

When *Rosa26*-LSL-*Ngf*-IRES-eGFP mice were crossed to KPC mice to generate KPCN mice, *Ngf* overexpression led to prominent perineural invasion (Figure 4O) and enlarged intratumoral nerves (Figure 4P). Furthermore, *Ngf* overexpression accelerated tumor formation and reduced median OS compared to regular KPC mice (13 weeks vs. 19 weeks) (Figure 4Q).

We investigated compartment-specific expression patterns of NTs in human PDAC using laser capture microdissection technique (LCM). LCM specimens were collected from 60 paired epithelial and stromal samples and gene expression analyzed using RNA-seq (Figure S4G). The pattern of NT expression in human PDAC showed marked differences from murine PDAC, as *BDNF* was expressed in 52% of the epithelial samples. In comparison, *NGF* was highly expressed in only 2% of the 60 cases (Figure S4H). Nevertheless, when human Panc-1 cells were stimulated with NE, both *BDNF* and *NGF* mRNA were upregulated, although *BDNF* was expressed at a much higher level (100-fold) (Figure S4I). The upregulation of *NGF* was also reversed by ICI, and by either KT5720 or U0126 (Figure S4J). ELISA confirmed that treatment with NE led to significantly increased NGF and BDNF secretion (Figure S4K). Similar to murine cells, this phenomenon was not reversed by atenolol but blocked by ICI, KT5720, and U0126, arguing again for the PKA and ERK downstream pathways mediating in part NT secretion in human PDAC cells.

In a complimentary experiment, Panc-1 cells were treated with Forskolin, an activator of adenylate cyclase, and PMA (Phorbol 12-myristate 13-acetate), an activator of protein kinase C (PKC) and the ERK pathway. While Forskolin and PMA alone were unable to stimulate NTs, combined treatment with Forskolin and PMA increased significantly NGF and BDNF secretion (Figure S4L). In contrast, NE - dependent increase in NT secretion was not blocked by SB203580 (specific inhibitor of p38-MAPK), BAY11-7085 (NF-κB inhibitor) or LY-294002, a strong inhibitor of phosphoinositide 3-kinases (Figure S4M). Taken together, similar to the murine models, adrenergic signaling stimulates NT secretion from human PDAC cells through the ADRB2 and PKA/ERK pathways.

Blockade of NGF/Trk Pathway Inhibits Proliferation and Innervation and Increases Overall Survival in KPC Mice

To clarify the contribution of increased NGF levels to pancreatic tumor growth *in vivo*, we employed the pan-Trk inhibitor, PLX-7486 (PLX) (Hayakawa et al., 2017). NGF has been shown to stimulate proliferation of PDAC cell lines (Dang et al., 2006), and the NGF-TrkA interaction is important in promoting growth and invasion of PDAC (Zhu et al., 1999). Murine PDAC cells express Trk receptors (Figure 5A) and PLX is able to block NGF-dependent stimulation of their proliferation (Figure 5B), indicating some role for direct effects on tumor growth by NGF. There are slight differences between the responses of the two KPC cell lines, with K2548 showing a higher response to 500 nM of NGF and K8282 showing baseline inhibition of cell viability with PLX alone, suggesting the possibility of baseline autocrine signaling. PLX also reduced sphere number, with or without ISO stimulation, below basal levels (Figure S5A).

The direct effects of NGF were clearly independent of ADRB2 signaling, since NGF stimulation of KPC sphere growth was not inhibited by pretreatment with ICI (Figure S5B)

or by deletion of the *Adrb2* (Figure S5C). In contrast, treatment of KC-*Adrb2* KO spheres with PLX inhibited both basal and NGF-induced stimulation of sphere numbers. Taken together, these results support an autocrine effect of NGF/Trk signaling that is independent of ADRB2. To assess the indirect actions of Trk blockade on tumor proliferation through inhibition of neurite outgrowth, we employed the co-culture model and measured neurite outgrowth using confocal imaging. Treatment of co-cultures with PLX significantly suppressed outgrowth of neurites from DRGs at 6 and 10 days (Figures S5D-F).

The effect of PLX on the incidence and growth of pancreatic tumors *in vivo* was investigated in two mouse models (KC and KPC) in which Trk receptors are expressed (Figure 5C). The cerulein-treated KC mouse was used as an additional PDAC model, since the marked inflammatory state following cerulein-induced pancreatitis leads to accelerated PDAC development (Figure S5G). In this inflammation driven PDAC model, PLX treated KC mice (Cer PLX) showed reduced proliferative activity with significantly fewer $Ki67^+$ cells/slide (Figure 5D), and roughly ten times more normal acinar tissue in comparison to KC mice on control diet (Cer) (Figure 5E). When this model was carried out to 24 weeks (Figure S5H) the cancer incidence of 60% in cerulein treated KC mice was significantly decreased to 10% in KC mice, receiving PLX-7486. (Figure S5I).

We next performed an interventional survival study in KPC mice, enrolling animals with tumor diameter from 3-6 mm and treating them with either GEM biweekly or GEM and PLX (GEM PLX). Combination treatment with GEM PLX extended the OS of KPC mice from 32 days to 45 days (Figure 5F). Immunostaining for peripherin revealed a significant reduction in nerve area in PDAC of KPC mice treated with GEM PLX, consistent with a decrease in NGF signaling (Figure 5G). Furthermore, administration of PLX and ICI along with GEM biweekly to KPC mice with pancreatic tumors between 20-60 mm^3 resulted in an OS of 47 days (Figure S5J). While the overall survival of this triple therapy cohort appeared to be greater than that observed with the GEM ICI treated animals (31 days, Figure 2G), the groups cannot be directly compared since they were not part of the same randomized study. Thus, while preliminary findings suggest the possibility of an additional NGF autocrine effect, further work is needed to determine if the triple combination provides significant additional benefit.

Nonselective β-Blocker Treatment Increases Overall Survival in Surgically Resected PDAC Patients

To clarify the relevance of ADRB2 signaling and nerve-cancer interactions in human PDAC, we studied 3D primary human PDAC organoids (Reichert et al., 2013). After 6 days of treatment with GEM (IC_{50}: 20.95 nM), fewer relative light units (RLU) were seen after treatment in all three organoid lines (Figures 6A and B). The administration of propranolol also caused a significant decrease in RLU. This was further enhanced when GEM and propranolol were combined. The addition of ICI, but not atenolol to the cultures caused a significant decrease in RLU (Figures S6A and B).

To determine whether there was a correlation between ADRB2 blockade and clinical outcome in PDAC, we retrospectively analyzed a cohort of patients resected for stage II and III PDAC at the University of Munich and the University of Bologna between 2002 and

2013. Patients receiving no β-blockers (NBB) during the postoperative follow-up had a median OS of 23 months. When these patients were compared to patients receiving any β-blocker treatment (β1-selective; SB1B and nonselective β-blocker; NSBB) there was no significant difference (23 vs. 24 months) (Figure 6C). However, when we compared patients that had NSBB (propranolol, carvedilol or sotalol) to patients that had NBB, the OS was nearly doubled (40 vs. 23 months) (Figure 6D). There was no difference in OS for patients that had SB1B (20.3 months). Patient characteristics, apart from a higher cardiovascular risk profile in patients on any β-blocker therapy, were comparable between groups. Patients were also similar in terms of primary tumor location, surgical procedures, postoperative complications, and adjuvant therapy, as tumor stage was not significantly different. There was also no difference in the resection status between groups. Only a minority of patients received neoadjuvant therapy (4-6% in each group).

Analysis of ADRB2 expression in human PDAC samples (Figure S6C) revealed epithelial expression of this protein. We performed staining for the neuronal marker S-100 on tumor sections from NBB patients, SB1B patients and NSBB patients (Figure 6E). In the NSBB group, we found fewer S-100^{+} intratumoral structures compared to NBB or SB1B patients. There was a trend towards a lower perineural invasion/nerve ratio in the NSBB group. Similarly, there was decreased staining for BDNF in tumor sections from NSBB patients compared to NBB or SB1B patients (Figure 6F). The positive and negative controls for the BDNF antibody used are depicted in Figures S6D-G. Taken together, patients with stage II/III PDAC undergoing surgery appear to have lower BDNF levels, reduced nerve density, and better survival when taking nonselective β-blockers.

Discussion

Here, we demonstrate a crosstalk between adrenergic signaling and cancer-derived NT secretion that is central to growth of PDAC. Elevated circulating catecholamines associated with chronic stress induce increased secretion of NGF or BDNF, which leads to axonogenesis through Trk receptors and further increased adrenergic input into the tumor microenvironment. ADRB2 and/or Trk inhibition interrupts this cross talk, inhibits stress-induced innervation and pancreatic tumorigenesis, and prolongs survival in KPC mice. Collectively, this data describes a feed-forward loop in which sustained adrenergic signaling can stimulate NTs and promote tumor innervation with subsequent increased NE accumulation and enhanced tumor growth.

Emerging evidence has pointed to innervation as a critical factor in the microenvironment that contributes to the growth of a variety of malignancies (Kiberstis, 2017; Monje, 2017). While gastric cancer is clearly stimulated by cholinergic signaling, recent studies in mice showed that in PanINs, sensory innervation increased dramatically, contributing to invasive tumor spread (Stopczynski et al., 2014), which can be inhibited by ablation of sensory neurons (Saloman et al., 2016). Sensory nerves may contribute to PDAC progression in part through direct signaling to neoplastic neuroendocrine cells expressing the substance P (SP) receptor Neurokinin 1-R (NK1-R) (Sinha et al., 2017). Nevertheless, our current study demonstrates that stress-dependent sympathetic signaling can induce PDAC in preneoplastic lesions (i.e. PanINs), and thus cancer development in a susceptible host could be inhibited

by ADRB2-antagonists. ADRB2 signaling likely promotes tumorigenesis through effects on both the epithelial and the stromal compartment (Hayakawa and Wang, 2017; Magnon et al., 2013; Zahalka et al., 2017). Although the effects of stress in promoting cancer have been linked in the past to suppression of the immune response (Partecke et al., 2016) or to recruitment of M2 macrophages (Madden et al., 2011; Pérez Piñero et al., 2012), we show here that many of the effects of circulating catecholamines are indeed direct, with stimulation of ADRB2-dependent pancreatic epithelial growth.

The role of β-adrenergic signaling in PDAC progression is supported by our retrospective clinical study, which demonstrated a significantly improved OS in patients on non-selective beta blockers (NSBB), although the analysis was limited by the uncertain duration and dosage of β-blockers. As shown, the vast majority of patients who undergo surgery for PDAC are currently treated with NBB or SB1B. β1-selective drugs provide no clinical advantage, consistent with our *in vitro* studies showing that atenolol did not suppress proliferation of *Kras* mutant pancreatic cells. Among the 2394 patients in a very recent study (Udumyan et al., 2017), only 21 were NSBB patients. Nevertheless, patients who used β-blockers (n=522) had a lower cancer-specific mortality rate than nonusers. No clear rate differences were observed by β-blocker receptor selectivity owing to very few patients on NSBB. A SEER-Medicare analysis also showed improved survival in patients with PDAC on β-blocker therapy (Beg et al., 2017).

Although a role for adrenergic signaling in cancer has been suspected, we report here in murine PDAC models a feed-forward signaling loop, whereby ADRB2-signaling leads to upregulation of NGF secretion, thus fueling increased axonogenesis and tumor growth. In PDAC, NGF secretion was clearly downstream of both the ADRB2 and PKA pathways, as blockade of ADRB2 or knockout of *Adrb2* or use of a PKA inhibitor reduced NGF expression and secretion. Our data indicates that there is likely a basal level of NGF secretion or Trk signaling, independent of adrenergic stimulation, which mediates an autocrine effect and can be inhibited by PLX.

In contrast to the predominance of NGF in mice, BDNF was the most abundant NT in human PDAC epithelium, consistent with a previous report (Miknyoczki et al., 1999). Although TrkA is the primary receptor for NGF, TrkB is the major receptor for BDNF, but importantly both of these receptors are inhibited by PLX-7486. TrkB acts as a potent suppressor of anoikis, which is associated with the acquisition of an aggressive tumorigenic and metastatic phenotype *in vivo* (Douma et al., 2004). Interestingly, the stromal compartment is also an important source of NTs. *BDNF* was expressed in 35% and *NTF3* in 15% of stromal compartments derived from human PDAC. The expression of NT/axonal guidance molecules in the stromal compartment is consistent with enhanced axonogenesis in pancreatic tumorigenesis, and the survival benefit observed with Trk inhibition.

Previous reports noted that expression of NGF starts to increase even at a premalignant stage of a genetically engineered mouse model of PDAC, suggesting the existence of an early axonogenic influence on tumorigenesis (Stopczynski et al., 2014). It is also known that NTs are involved in axonal guidance (Gillespie, 2003). Additionally, genomic analysis of human PDAC revealed frequent and diverse somatic aberrations in embryonic regulators of axon

guidance, particularly SLIT/ROBO signaling (Biankin et al., 2012), supporting a role for neural modulation in pancreatic carcinogenesis. The cancer associated fibroblast (CAF)-secreted SLIT2 increases neurite outgrowth from dorsal root ganglia, so that inhibition of SLIT2/ROBO signaling disrupts this stromal/neural connection (Secq et al., 2015).

Overexpression of *Ngf* in the epithelial compartment led to expansion of nerves, accelerated pancreatic tumor development, and decreased survival in our mouse models, demonstrating a clear functional role for axonogenesis in PDAC. Moreover, blocking Trk receptors inhibited tumorigenesis in the KC mouse, and in combination with GEM slowed axonogenesis and tumor development, and prolonged survival in the KPC mouse. When a Trk inihibitor was added to ADRB2-blockade, survival of KPC mice appeared to be enhanced, arguing for a tumor-promoting autocrine effect of NTs that was abrogated in by NGF/Trk inhibition. Furthermore, our clinical data suggests lower BDNF levels, reduced nerve density and better survival in PDAC patients on NSBB. These results suggest that remodeling of the nervous system contributes to all stages of PDAC, including those that precede the appearance of cancer.

In summary, this study in PDAC exemplifies the important role of nerves in the development of cancer. In the case of PDAC, we have shown the important role at early stages of PDAC development for systemic stress and elevated catecholamine levels. Our findings suggest that blocking either ADRB2 and/or Trk receptors represents a promising preventive or therapeutic strategy for PDAC, a disease for which more effective approaches are urgently needed.

STAR★METHODS

KEY RESOURCES TABLE

REAGENT or RESOURCE	SOURCE	IDENTIFIER
Antibodies		
Rabbit polyclonal anti-ADRB2	Abcam	Cat#ab36956; RRID: AB_867831
Rabbit polyclonal anti-Peripherin	EMD Millipore	Cat#AB1530; RRID: AB_90725
Rabbit polyclonal anti-Norepinephrine	Abcam	Cat#ab8887; RRID: AB_306840
Rabbit polyclonal anti-Ki67	Abcam	Cat#ab15580; RRID: AB_443209
Rabbit polyclonal anti-pan TRK	Abcam	Cat#ab79770; RRID: AB_1603910
Rabbit monoclonal anti-S100B	Dako	Cat#Z0311; RRID: AB_10013383
Rabbit monoclonal anti BDNF	Abcam	Cat#ab108319; RRID: AB_10862052
Rabbit polyclonal anti-GAP43	Invitrogen	Cat#PA1-16729; RRID: AB_568546
Rabbit polyclonal anti-Tyrosine Hydroxylase	EMD Millipore	Cat#AB152; RRID: AB_390204
Rabbit monoclonal anti-phosphorylated ERK	Cell Signaling Technology	Cat#9101S; RRID: AB_331646
Rabbit polyclonal anti-ERK	Cell Signaling Technology	Cat#4695S; RRID: AB_390779
Rabbit monoclonal anti-phosphorylated CREB	Cell Signaling Technology	Cat#9198S; RRID: AB_2561044

REAGENT or RESOURCE	SOURCE	IDENTIFIER
Rabbit monoclonal anti-CREB	Cell Signaling Technology	Cat#9197S; RRID: AB_331277
Rabbit monoclonal anti-phosphorylated p38	Cell Signaling Technology	Cat#4511S; RRID: AB_2139682
Rabbit polyclonal anti-phosphorylated YAP	Cell Signaling Technology	Cat#4911S; RRID: AB_2218913
Rabbit monoclonal anti-phosphorylated IκBα	Cell Signaling Technology	Cat#2859S; RRID: AB_561111
Rabbit polyclonal anti-β Actin	Cell Signaling Technology	Cat#4967S; RRID: AB_330288
Rat APC anti-mouse CD326 (Ep-CAM)	BioLegend	Cat#118214; RRID: AB_1134102
Biotynilated goat anti-rabbit IgG	Vector Laboratories	Cat#BA-1000; RRID: AB_2313606
Donkey Anti-Rabbit IgG, HRP-Linked Whole Ab	GE Healthcare Life Sciences	Cat#NA-934; RRID: AB_772206
Chicken anti-Rabbit, Alexa Fluor 488	Invitrogen	Cat#A-21441; RRID: AB_141735
Bacterial and Virus Strains		
Ad5CMVCre	Viral vector Core, The University of Iowa	Cat#VVC-U of Iowa-5
Biological Samples		
Human pancreatic cancer samples	Columbia university	N/A
Human pancreatic cancer samples	University of Munich	N/A
Chemicals, Peptides, and Recombinant Proteins		
Isoproterenol hydrochloride	Sigma-Aldrich	Cat#I5627; CAS: 51-30-9
DL-Norepinephrine hydrochloride	Sigma-Aldrich	Cat#A7256; CAS: 55-27-6
Atenolol	Sigma-Aldrich	Cat#A7655; CAS: 29122-68-7
Propranolol hydrochloride	Sigma-Aldrich	Cat#P0884; CAS: 318-98-9
ICI 118,551	Tocris	Cat#0821; CAS: 72795-01-8
KT5720	Sigma-Aldrich	Cat#K3761; CAS: 108068-98-0
U0126	Promega	Cat#V1121; CAS: 109522-58-2
LY294002	Sigma-Aldrich	Cat#L9908; CAS: 934389-88-5
BAY11-7085	Sigma-Aldrich	Cat#B5681; CAS: 196309-76-9
SB203580	Sigma-Aldrich	Cat#S8307; CAS: 152121-47-6
Forskolin	Sigma-Aldrich	Cat#F3917; CAS: 66575-29-9
PMA	Sigma-Aldrich	Cat#P1585; CAS: 16561-29-8
Human β-NGF	PeproTech	Cat#450-01
Murine β-NGF	PeproTech	Cat#450-34
gemcitabine	LC Laboratories	Cat#G4177
PLX-7486	Plexxikon	N/A
Cerulein	Sigma-Aldrich	Cat#C9026
N-2 Supplement	Gibco	Cat#17502048
B-27 Supplement	Gibco	Cat#17504044
Nu-serum IV	Corning	Cat#355104
Cholera Toxin from *Vibrio Cholerae*	Sigma-Aldrich	Cat#C8052, CAS 9012-63-9
Trypsin Inhibitor from *Glycine Max*	Sigma-Aldrich	Cat#T6522, CAS 9035-81-8
Collagenase Type V	Sigma-Aldrich	Cat#C9263, CAS 9001-12-1

REAGENT or RESOURCE	SOURCE	IDENTIFIER
Trypsine 0.05%	Gibco	Cat#25300054
DAPI Solution	BD Pharmingen	Cat#564907
ACK Lysing Buffer	Gibco	Cat#A1049201
HBSS – Hank's Balanced Salt Solution	Gibco	Cat#14175079
Normal Goat Serum Blocking Solution	Vector Laboratories	Cat#S-1000
VECTASHIELD Antifade Mounting Medium with DAPI	Vector Laboratories	Cat#H-1200
Leivobitz's L-15	Gibco	Cat#11415064
Matrigel Matrix	Corning	Cat#356234
RPMI Medium 1640	Gibco	Cat#11875093
DMEM	Gibco	Cat#11995065
Fetal Bovine Serum	Gibco	Cat#16140071
DPBS, no calcium, no magnesium	Gibco	Cat#14190250
Bovine Serum Albumin	Sigma-Aldrich	Cat#A9418
TritonX-100	Fisher Scientific	Cat#BP151-500
TWEEN 20	Sigma-Aldrich	Cat#P1379
Dimethyl Sulfoxide	Sigma-Aldrich	Cat#D8418
Penicillin Streptomycin	Gibco	Cat#15140122
Critical Commercial Assays		
Mouse β-NGF ELISA kit	RayBiotech	Cat#ELM-bNGF-1
Human β-NGF ELISA kit	R & D	Cat#DY256-05
Human BDNF ELISA kit	Sigma-Aldrich	Cat#RAB0026
MTT Cell Proliferation Assay Kit	invitrogen	Cat#V13154
SuperScript III First-Strand Synthesis System	Invitrogen	Cat#18080051
SYBR Green Master Mix	Applied Biosystems	Cat#A25742
Alzet pump model 2004	DURECT Corporation	Cat#2004
VECTASTAIN ABC HRP kit	Vector laboratories	Cat#PK-4000
Liquid DAB+ Substrate Chromogen System	Dako	Cat#K3468
RNA*later* stabilization solution	Ambion	Cat#AM7020
NucleoSpin RNA kit	Macherey-Nagel	Cat#740955
RNAqueous-micro kit	Ambion	Cat#AM1931
ECL Western Blotting Detection Reagents	Amersham	Cat#RPN2209
RNeasy Micro Kit	QIAGEN	Cat#74004
Ovaton RNA-Seq System V2	NuGEN	Cat#7102
Deposited Data		
Human RNAseq data	This paper	GEO: GSE93326
Experimental Models: Cell Lines		
Human: AsPC-1 cells	ATCC	CRL-1682
Human: BxPC-3 cells	ATCC	CRL-1687

REAGENT or RESOURCE	SOURCE	IDENTIFIER
Human: MIA PaCa-2 cells	ATCC	CRL-1420
Human: Panc-1 cells	ATCC	CRL-1469
Mouse: K8282 cells	This paper; provided from Dr. Kenneth P. Olive	N/A
Mouse: K2548 cells	This paper; provided from Dr. Kenneth P. Olive	N/A
Experimental Models: Organisms/Strains		
Mouse: *Pdx1*-Cre	Hingorani et al., 2005; provided from Dr. Kenneth P. Olive	N/A
Mouse: LSL-*Trp53*$^{+/R172H}$	Hingorani et al., 2005; provided from Dr. Kenneth P. Olive	N/A
Mouse: LSL-*Kras*$^{+/LSL-G12D}$	Hingorani et al., 2005; provided from Dr. Kenneth P. Olive	N/A
Mouse: *Adrb2* knockout: *Adrb1*^{tm1Bkk} *Adrb2*^{tm1Bkk}/J	The Jackson Laboratory	Stock No: 003810
Mouse: *Rosa26*-LSL-*Ngf*-IRES-EGFP	Hayakawa et al., 2017	N/A
Mouse: mTmG mouse: B6.129(Cg)-*Gt(ROSA)26Sor*$^{tm4(ACTB-tdTomato,-EGFP)Luo}$/J	The Jackson laboratory	Stock No: 007676
Oligonucleotides		
Primers for qRT-PCR, see Table S1.	This paper	N/A
Software and Algorithms		
ImageJ Fiji (version 2.0.0-rc44)	N/A	https://fiji.sc/
Prism 7 for Mac OS X	GraphPad Inc.	http://graphpad.com
FlowJo (version 10)	FlowJo	https://www.flowjo.com

CONTACT FOR REAGENT AND RESOURCE SHARING

Further information and requests for resources and reagents should be directed to and will be fulfilled by the Lead Contact, Timothy C. Wang (tcw21@columbia.edu).

EXPERIMENTAL MODEL AND SUBJECT DETAILS

Mouse models—All animal experiments were conducted in compliance with the National Institute of Health guidelines for animal research and approved by the Institutional Animal Care and Use Committee of the Columbia University. Mice were housed in a specific pathogen-free facility. A Pdx1 driver strain was used to activate a conditional lox-stop-lox-*Kras*^{G12D} and a conditional lox-stop-lox-*Trp53*^{R172H} allele as previously described (Hingorani et al., 2005). A cohort of *Kras*$^{+/LSL-G12D}$;*Pdx1*-Cre (KC) mice was also crossed onto a *Adrb2* knockout allele (Chruscinski et al., 1999). Another cohort of KC mice was crossed onto a *Rosa26*-LSL-*Ngf*-IRES-eGFP allele (Hayakawa et al., 2017) in order to overexpress *Ngf* restricted to the pancreas with an oncogenic *Kras* mutation. B6.129(Cg)-*Gt(ROSA)26Sor*$^{tm4(ACTB-tdTomato,-EGFP)Luo}$/J mice (mTmG mice, Jackson Laboratories) were used for immunohistochemical staining and for the isolation of the dorsal root ganglia.

Human tissue samples—Human pancreatic cancer samples for RNA-seq analysis were obtained from Columbia University. Human pancreatic cancer samples for staining were obtained from the University of Munich (Dr. Jens Neumann, Dept. of Pathology). Human pancreatic cancer samples for organoid cultures were obtained from the Technische Universität München (Dr. Maximilian Reichert, Dept. of Medicine II). All samples were anonymized. All protocols using human materials were approved by the ethics committee of the Columbia University, the University of Munich or the Technische Universität München. Written informed consent was obtained from all patients.

Cell line culture—All human pancreatic cancer cell lines were purchased from ATCC. Murine pancreatic cancer cell lines derived from KPC mice were provided from Dr. Kenneth P. Olive. All cell lines were cultured in RPMI-1640 medium (supplemented with 10% FBS and 1% penicillin/streptomycin in a humidified incubator at 37 °C, as described previously (Hayakawa et al., 2011).

METHOD DETAILS

Restraint stress model—Immobilization stress, which mimicked the presence of a natural predator without possibility of escape, was created by placing mice into a 50 ml conical vial with openings for breathing. Vials with mice were placed for 6 hr in a plastic box that contained tissue impregnated with fox urine (Chagnon's Trapping Supply). The ADRB2 antagonist ICI 118,551 (Tocris) (0.2 μg/g) was given intraperitoneally 30 min before immobilization stress. To avoid unintended stress, mice were handled with extra care. Manipulations that could cause distress (e.g., injections and blood sampling) were conducted under light isoflurane anesthesia (Hassan et al., 2013).

Surgical procedures

Ganglionectomy (Gx): Eight-week-old KC mice, were anesthetized using isoflurane. A mixture of Lidocain (10 μg/g) and Bupivacain (5 μg/g) was injected subcutaneously along the incision line. A midline laparotomy allowed exteriorization of the pancreatic tail after mobilizing the spleen. After dissecting the pancreas until the level of the portal vein, the celiac artery and the superior mesenteric artery (AMS) were identified. The nerve bundles around the celiac axis and between the celiac artery and the AMS were subtly resected using micro-surgical instruments under an operating microscope (25× magnification). After careful irrigation of the entire abdominal cavity with 0.9% sterile and pre-warmed saline, the situs was checked for cessation of bleeding and the procedure was ended by closing the abdominal muscles using 5-0 vicryl sutures (Ethicon), and the skin was stapled using 9.0-mm staples (Reflex Skin Closure Systems). Carprofen (Rimadyl® 5 mg/g) was injected intraperitoneally before surgery and the next day.

Bilateral adrenalectomy (ADx): Eight-week-old KC mice were anesthetized using isoflurane. A mixture of Lidocain (10 μg/g) and Bupivacain (5 μg/g) was injected subcutaneously along the incisions line. A longitudinal skin incision was made above the spine and then lateral incisions in the muscle wall to access the adrenals. The adrenal artery and veins were identified and cauterized using a battery driven high temperature heat cautery (FST) or ligated using 9/0 non-absorbable microsutures (S&T Swaged Microsurgical

Sutures). Then the adrenals were dissected free and removed. After careful irrigation of the entire situs with 0.9% sterile and pre-warmed saline, the situs was checked for cessation of bleeding and the procedure was ended by closing the muscle wall using 5-0 vicryl sutures (Ethicon), and the skin was stapled using 9.0-mm staples (Reflex Skin Closure Systems). Carprofen (Rimadyl® 5 mg/g) was injected intraperitoneally before surgery and the next day.

Osmotic pump implantation: Eight-week-old KC mice, were anesthetized using isoflurane. A skin incision was made on the back of the animals and a hemostat was inserted into the incision, and, by opening and closing the jaws of the hemostat, a subcutaneous pocket for the pump was created. The isoproterenol (10 μg/g/day) filled pumps (Alzet pumps model 2004, DURECT Corporation) were replaced every 28 days. Carprofen (Rimadyl® 5 mg/g) was injected intraperitoneally before surgery.

Mice treatment—KPC mice were palpated for any mass in the pancreas. Once there was a tumor suspected, they were screened by VEVO 2100 Ultrasound Imaging System (FUJIFILM VisualSonics) for pancreatic cancer. Tumor volume (V) was determined by the following formula: V = (long diameter)×(short diameter)×(short diameter)/2. Gemcitabine (100 mg/kg) was intraperitoneally injected biweekly. ICI 118,551 (0.2 μg/g) was intraperitoneally injected daily. PLX-7486, provided from Plexxikon, has been used in Phase I clinical studies and detailed information is available on the NCI drug dictionary: http://www.cancer.gov/publications/dictionaries/cancer-drug?cdrid=747694. PLX-7486 was mixed into the AIN-76A mouse chow (100 mg/kg), and fed for the indicated periods. The control group was given AIN-76A chow without PLX-7486. Mice were randomly assigned to each treatment group and followed-up weekly by ultrasound after enrollment for tumor volume measurement.

KC mice at 6-7 weeks were fasted overnight and subjected to seven hourly intraperitoneal injections of cerulein (Sigma-Aldrich) (50 μg/kg) on two consecutive days. Mice were sacrificed 12 or 16 weeks after the last dose of cerulein.

Histology, immunohistochemistry and immunocytochemistry—Following isoflurane inhalation, blood was immediately collected into serum collection vials (BD Biosciences) by retro-orbital venous plexus puncture, and mice were then euthanized by cervical dislocation. The pancreas was removed. The organ was fixed overnight in 10% phosphate-buffered formalin or 4% paraformaldehyde, and embedded into paraffin block or OCT compounds, respectively. Histological scoring was performed according to published criteria by board certified gastrointestinal pathologists (A.C.I.), who were blinded as to sample identity.

4 μm paraffin embedded sections were prepared for immunohistochemistry. For immunohistochemical staining of murine samples, slides were first deparaffinized in xylene. Endogenous peroxidase was blocked by incubation with 3% hydrogen peroxide in methanol for visualization using the peroxidase reaction. Antigen retrieval was performed by boiling the slides in citrate buffer (10 mM, pH 6.0) in a water bath for 20 min. Slides were rinsed in PBS Tween 0.05% and blocked for 30 min with 2% bovine serum albumin (BSA) or 10%

normal goat serum (Vector Laboratories). Primary antibodies and biotinylated secondary antibodies (Vector Laboratories) were diluted in 2% BSA. Slides were incubated overnight at 4°C with primary antibodies and for 30 min at room temperature with secondary antibodies. Subsequently, slides were incubated with peroxidase conjugated avidin (Vector Laboratories) and 3,3′-diaminobenzidine (Dako) as a chromogen. Slides were counterstained with hematoxylin and mounted for viewing.

For frozen sections, slides were permeabilized with 0.5% TritonX-100 in PBS and blocked with 1% BSA for 1 hr. Primary antibodies were applied for overnight staining. Alexa Fluor 488 secondary antibody (Invitrogen) was used to reveal the staining. Slides were counterstained and mounted with a mounting medium with DAPI (Vector Laboratories).

For immunocytochemistry, cells were washed with PBS and fixed using 10% neutral buffered formalin. Cells were immuno-stained according to the standard protocol. Bright field and fluorescence images were acquired using an Eclipse TU2000-U microscope (Nikon) connected to a cooled color CCD camera (RTKE Diagnostic Instruments) using SPOT software. A complete list of antibodies is given in KEY RESOURCES TABLE. Stained area was quantified by ImageJ using color deconvolution mode.

All immunohistochemical stainings on human samples were done on 4 μm whole standard tissue sections of formalin fixed, paraffin embedded (FFPE) tumor samples. The staining was performed on a Ventana Benchmark XT autostainer using the XT UltraView diaminobenzidine kit (Ventana Medical Systems).

Scoring of staining intensity was done as previously described (Myers et al., 1994). Briefly, if staining intensity was equal to the control normal adjacent pancreatic tissue the specimen was considered negative (0); immunostaining greater than the control normal adjacent pancreatic tissue, but limited to less than 25% of the cells in a tissue section, was scored as weak (1); immunostaining intensity greater than the control, and present in less than 50% of the cells, was scored as moderate (2); and immunostaining intensity greater than the control and present in more than 50% of the cells was scored as strong (3).

For quantification of nerve area, 5 slides/animal were stained for peripherin 200 μm apart and quantified by measuring nerve number/mm^2 tissue section (neural density) and positively stained area in percent of the entire section (neural hypertrophy).

For scoring murine pancreatic intraepithelial neoplasia (PanIN), PanIN was scored based on the degree of cytological atypia and epithelial proliferation. Microinvasion was also identified in association with foci of small duct intraepithelial neoplasia. The majority of small duct intraepithelial neoplasia in the KC consists of flat neoplastic lesions with: 1. mucinous epithelial lining with minimal cytological atypia (PanIN-1), 2. atypical epithelial lining with preserved nuclear polarity (PanIN-2) and 3. Intraductal epithelial proliferation filling and expanding small ducts, showing severe cytological atypia, loss of polarity, increased mitotic activity, nuclear enlargement with irregular contours and hyperchromasia (PanIN-3). Ten consecutive ductal areas were scored for small duct intraepithelial neoplasia. Nodular clusters of coalescing small ducts expanded by solid neoplastic epithelial proliferation were seen. These microcarcinomas showed foci of microinvasion and were also

seen adjacent to larger poorly differentiated carcinomas. The number of microcarcinomas was assessed on full-face sections of the entire mouse pancreas. The larger pancreatic ducts showed mucinous epithelial lining and scattered foci of papillary and micropapillary proliferation with variable degree of cytological atypia. The pancreas adjacent to the intraepithelial neoplasia displays acinar-ductal metaplasia and acinar atrophy.

Murine and human pancreatic spheres—We isolated single cells from adult mouse pancreas or human pancreatic cancer tissue and cultured 3D spheroid cysts based on the protocol previously reported (Reichert et al., 2013). After the tissue was harvested, it was chopped into small pieces and digested in 1 mg/ml collagenase-V (Sigma-Aldrich) at 37 C° for 20 min. Following multiple washes with Hank's balanced salt solution (HBSS, Gibco) supplemented with 5% fetal bovine serum (FBS), collagenase-digested pancreatic tissue was spun down. The pellet was then diluted in trypsin-EDTA (0.05%) (Gibco) and incubated at room temperature for 5 min. After multiple washes, cells were filtered through a 40 μm cell strainer. Cells were resuspended in Matrigel (Corning) with or without Adeno-Cre virus (provided from the University of Iowa), and 6.5×10^3 cells/well were seeded into a pre-warmed 24 well plate. Cells were cultured in DMEM (Gibco) containing B27 and N2 supplements (Gibco), 5% Nu-Serum IV (Corning), 100 μg/ml trypsin inhibitor, and 100ng/ml Cholera Toxin (Sigma-Aldrich). Medium was replaced every other day. Sphere number and diameter was measured on day 5-7 using ImageJ software.

Dorsal root ganglia isolation and co-culture—Embryos (E14.5) from timed pregnant C57BL/6 mice or B6.129(Cg)-*Gt(ROSA)26Sor*$^{tm4(ACTB-tdTomato,-EGFP)Luo}$/J mice for imaging purposes on the 14th day of gestation were utilized for dorsal root ganglia isolation. Following isoflurane inhalation, mice were euthanized by cervical dislocation. The mother mouse was placed in supine position and the abdomen thoroughly sprayed with 70% ethanol and an abdominal midline incision was made. The uterus laden with embryos was grasped with forceps near cervical insertion and gently lifted from peritoneal cavity. Connective tissue and suspensory ligaments were cut away and the entire uterus was placed in a sterile 10 cm tissue culture dish. From here the procedure was perfomed in a dissection hood. Embryos were removed from the uterus by cutting through tissue surrounding amniotic fluid and gently squeezing embryo through incision. All embryos were placed into another 10 cm dish containing L-15 (Gibco) in order to "clean" the embryos. Individual embryos are transferred to a 6 cm dish with a thin layer of L-15 to isolate DRGs. The embryo is laid on its side and, under a dissecting microscope, the head is cut off at the cervical flexure and the tail just caudal to the hind limbs using micro-dissecting scissors. The ventral portion of the embryo is removed to isolate the dorsal structures containing the spinal cord. One blade of micro-dissecting scissors is placed between the vertebral column and the spinal canal at rostral end and it is carefully cut through the vertebral column proceeding caudally. Then the right and left halves of vertebral column are teased apart to expose spinal cord and DRGs. The spinal cord is gently lifted from dorsal structures by grasping the cord at the rostral end while carefully "cutting" behind and around DRGs to sever adherent tissues. Once the entire spinal cord and the attached DRGs are freed, they are transferred to a clean 6 cm dish containing a thin layer of L-15. After isolating all spinal cords, the DRGs are plucked off

using dissecting forceps and transferred to another 6 cm dish with L-15. If nerve roots are present, they are snipped away before removing DRGs from cords.

For co-culture experiments murine pancreatic cancer cells or isolated spheres were resuspended in 25 μl Matrigel (Corning) and placed at exact 1 mm distance next to the to another 25 μl Matrigel dot.

One single DRG is then picked with forceps and placed on top of the “empty” 25 μl Matrigel dot. Both Matrigel suspensions are the carefully connected by a Matrigel bridge. The petri dishes were then placed for 20 min in an incubator set at 37 °C saturated with 5% before RPMI-1640 medium is added and replaced every other day. Pictures were taken on a Nikon A1RMP Nikon Ti Eclipse inverted multiphoton confocal microscope equipped with NIS-Elements software (Nikon). Outgrowth of neurites were measured by ImageJ using the simple neurite tracer (Longair et al., 2011).

Flow cytometry analysis and cell sorting—Murine pancreatic tumor was harvested, minced and digested as described in murine pancreatic spheres section with a longer digestion time (2 hr). Red blood cells were lysed (ACK Lysing Buffer) before passing through a 40 μm nylon mesh. Filtered single cells were incubated with EpCAM antibody (Biolegend). DAPI (4′,6-Diamidino-2-Phenylindole, Dihydrochloride) was used to exclude dead cells. Cells were sorted by FACSAria II (BD Biosciences) and used for subsequent experiments.

Proliferation assay—Cell proliferation was determined by the 3-(4,5-dimethyl-2-thiazolyl)-2,5-diphenyltetrazolium bromide (MTT) uptake method (Invitrogen). After the cells were seeded (5×10^3/well) in 200 μl of DMEM medium into 96-well plates and cultured overnight, isoproterenol, atenolol, ICI 118,551, propranolol, β-NGF (Peprotech), and PLX-7486 or their combination was added to the culture medium. After an incubation of 48 to 72 hr, MTT reagent (5 mg/ml) was added and incubation was continued for an additional 4 hr. The reaction was terminated with 150 μl dimethyl sulfoxide (DMSO, Sigma-Aldrich) per well. Absorbance values were determined using a 96-well multiscanner (Promega). The cells cultured in DMEM served as the control group. The cell viability index was calculated according to the following formula: experimental OD value/control OD value. The experiments were repeated three times.

Quantitative RT-PCR (qRT-PCR)—Total RNA was extracted from whole pancreas samples from each animal or cell cultures using RNA*later* stabilization solution (Ambion) and NucleoSpin RNA kit (Macherey-Nagel) or the RNAqueous-micro kit (Ambion) and subjected to first-strand complementary DNA synthesis using the Superscript III cDNA Amplification System (Invitrogen) following the manufacturer’s instructions. qRT-PCR was performed using a three-step method, an ABI 7300 system and SYBR green (Applied Biosystems). The qRT-PCR primer sequences are listed in Table S1. The results were expressed as the copy number of each gene relative to that of *Gapdh* or *GAPDH*.

Western blotting—Briefly, 5×10^5 cells were incubated on ice for 30 min in 0.5 ml of ice-cold whole-cell lysate buffer. Debris was removed by centrifugation. The protein content

of the cell was determined, and the cellular lysates were separated by 10% SDS-PAGE, and electro-transferred onto polyvinylidene difluoride membranes. After being blocked with 5% non-fat milk in TBST, the membranes were incubated with primary antibodies at 4 °C overnight, followed by 1:1000 horseradish peroxidase (HRP)-conjugated secondary antibody (GE Healthcare Life Sciences) for 1 hr. Immunoreactive bands were visualized using an enhanced chemiluminescence kit (Amersham). The Western blot signals were quantitated by densitometric analysis using ImageJ. Primary antibodies used are listed in KEY RESOURCES TABLE.

Enzyme-linked Immunosorbent assay (ELISA)—ELISA for murine β-NGF (RayBiotech), human β-NGF (R&D) and human BDNF (Sigma-Aldrich) were performed according to manufacturer's protocols.

Human RNA-seq analysis—Total RNA was isolated from the laser microdissected epithelial and stromal compartment of human pancreatic cancer using the RNeasy Micro kit (QIAGEN). cDNA was amplified, and libraries were prepared using the Ovation RNA-Seq System V2 (NuGEN). Sequencing was performed on the Illumnina HiSeq 2000 platform. Gene expression was quantified using 'Tophat' (Trapnell et al., 2009) with the NCBI/build 37.2 reference genome and 'HTSeq' (Anders et al., 2015) to obtain raw read counts per gene. Counts per library were converted to fragments per million mapped fragments (FPM) using the 'DESeq2' (Love et al., 2014) and R package (R Core Team, 2016, 2016). The number of samples per compartment with at least 1 FPM were counted for each of *NGF*, *BDNF*, *NTF3* and *NTF4* and were then categorized as 'detected'.

QUANTIFICATION AND STATISTICAL ANALYSIS

Statistical analysis—The means of two groups were compared using Student's t-test or Mann-Whitney u-test. Survival was compared using log rank testing. P values < 0.05 were considered to indicate statistical significance. All statistical analyses were performed using Prism 7 for Mac OS X (GraphPad Software, Inc.).

DATA AND SOFTWARE AVAILABILITY

RNA-seq data—The full RNA-seq data have been deposited in the Gene Expression Omnibus (https://www.ncbi.nlm.nih.gov/geo/) under an Accession Code GSE93326.

Supplementary Material

Refer to Web version on PubMed Central for supplementary material.

Acknowledgments

We thank Ms. Theresa Swayne for assistance with confocal microscopy. Images were collected in the Confocal and Specialized Microscopy Shared Resource at Columbia University, supported by NIH grant P30CA013696. The confocal microscope was purchased with NIH grant S10RR025686. These studies also used the resources of the Cancer Center Flow Core Facility funded in part through Center Grant P30CA013696. We further thank Ms. Wendy Beth Jackelow (Medical & Scientific Illustration) for creating schematic images, and Plexxikon Inc. for providing PLX-7486. This study utilized the Cancer Center Flow Core Facility funded in part through Center Grant P30CA013696. T. C. Wang received grants from the NIH (R35CA210088), the Pancreatic Cancer Action Network - ACCR (Innovative Grant) and the Lustgarten Foundation. B.W. Renz was supported by a German Research

Foundation grant (DFG RE3440/1-1). R. Takahashi and T. Tanaka were supported by Uehara Memorial Foundation. T. Tanaka was supported by the Japanese Society of Gastroenterology (JSGE). Y. Hayakawa was supported by the Project for Cancer Research and Therapeutic Evolution (P-CREATE) from the Japan Agency of Medical Research and Development, AMED. H.C. Maurer and M. Middelhoff were supported by a Mildred Scheel Postdoctoral Fellowship. C.B. Westphalen was supported by a German Research Foundation (DFG) grant. M. Reichert was supported by the National Pancreas Foundation (MR), the German Cancer Aid Foundation (Max Eder Program, Deutsche Krebshilfe 111273), the KKF Program (School of Medicine, Klinikum rechts der Isar, Technical University Munich), and the AGA-Actavis Research Award in Pancreatic Disorders. S.K. Mohanta was supported by a German Research Foundation grant (DFG MO3054/1-1). A. J.R. Habenicht was supported by a German Research Foundation grant (DFG HA1083/15-4). Finally, we express our greatest appreciation for Dr. Xiaowei Chen, an invaluable contributor and friend who sadly passed away in April of 2017.

References

Anders S, Pyl PT, Huber W. HTSeq—a Python framework to work with high-throughput sequencing data. Bioinformatics. 2015; 31(2):166–169. [PubMed: 25260700]

Apte MV, Wilson JS. Dangerous liaisons: pancreatic stellate cells and pancreatic cancer cells. J Gastroenterol Hepatol. 2012; 27(Suppl 2):69–74.

Bapat AA, Munoz RM, Von Hoff DD, Han H. Blocking Nerve Growth Factor Signaling Reduces the Neural Invasion Potential of Pancreatic Cancer Cells. PLoS ONE. 2016; 11:e0165586. [PubMed: 27792755]

Barron TI, Connolly RM, Sharp L, Bennett K, Visvanathan K. Beta blockers and breast cancer mortality: a population-based study. Journal of Clinical Oncology. 2011; 29:2635–2644. [PubMed: 21632503]

Batty GD, Russ TC, Stamatakis E, Kivimäki M. Psychological distress in relation to site specific cancer mortality: pooling of unpublished data from 16 prospective cohort studies. Bmj. 2017; 356:j108–j111. [PubMed: 28122812]

Beg MS, Gupta A, Sher D, Ali S, Khan S, Gao A, Stewart T, Ahn C, Berry J, Mortensen EM. Impact of Concurrent Medication Use on Pancreatic Cancer Survival-SEER-Medicare Analysis. Am J Clin Oncol. 2017

Benowitz LI, Routtenberg A. GAP-43: an intrinsic determinant of neuronal development and plasticity. Trends in Neurosciences. 1997; 20:84–91. [PubMed: 9023877]

Biankin AV, Waddell N, Kassahn KS, Gingras MC, Muthuswamy LB, Johns AL, Miller DK, Wilson PJ, Patch AM, Wu J, et al. Pancreatic cancer genomes reveal aberrations in axon guidance pathway genes. Nature. 2012; 491:399–405. [PubMed: 23103869]

Borden P, Houtz J, Leach SD, Kuruvilla R. Sympathetic innervation during development is necessary for pancreatic islet architecture and functional maturation. Cell Rep. 2013; 4:287–301. [PubMed: 23850289]

Ceyhan GO, Bergmann F, Kadihasanoglu M, Altintas B, Demir IE, Hinz U, Müller MW, Giese T, Büchler MW, Giese NA, et al. Pancreatic neuropathy and neuropathic pain–a comprehensive pathomorphological study of 546 cases. Gastroenterology. 2009; 136:177–186.e1. [PubMed: 18992743]

Ceyhan GO, Demir IE, Altintas B, Rauch U, Thiel G, Müller MW, Giese NA, Friess H, Schäfer KH. Neural invasion in pancreatic cancer: a mutual tropism between neurons and cancer cells. Biochem Biophys Res Commun. 2008; 374:442–447. [PubMed: 18640096]

Chruscinski AJ, Rohrer DK, Schauble E, Desai KH, Bernstein D, Kobilka BK. Targeted disruption of the beta2 adrenergic receptor gene. J Biol Chem. 1999; 274:16694–16700. [PubMed: 10358008]

Clark KL, Loscalzo M, Trask PC, Zabora J, Philip EJ. Psychological distress in patients with pancreatic cancer—an understudied group. Psycho-Oncology. 2010; 19:1313–1320. [PubMed: 20119937]

Collins MA, Yan W, Sebolt-Leopold JS, Pasca di Magliano M. MAPK signaling is required for dedifferentiation of acinar cells and development of pancreatic intraepithelial neoplasia in mice. Gastroenterology. 2014; 146:822–834.e827. [PubMed: 24315826]

Dang C, Zhang Y, Ma Q, Shimahara Y. Expression of nerve growth factor receptors is correlated with progression and prognosis of human pancreatic cancer. J Gastroenterol Hepatol. 2006; 21:850–858. [PubMed: 16704535]

Demir IE, Friess H, Ceyhan GO. Neural plasticity in pancreatitis and pancreatic cancer. Nat Rev Gastroenterol Hepatol. 2015; 12:649–659. [PubMed: 26460352]

Douma S, van Laar T, Zevenhoven J, Meuwissen R. Suppression of anoikis and induction of metastasis by the neurotrophic receptor TrkB. Nature. 2004

Gillespie LN. Regulation of axonal growth and guidance by the neurotrophin family of neurotrophic factors. Clin Exp Pharmacol Physiol. 2003; 30:724–733. [PubMed: 14516410]

Guerra C, Schuhmacher AJ, Cañamero M, Grippo PJ, Verdaguer L, Pérez-Gallego L, Dubus P, Sandgren EP, Barbacid M. Chronic Pancreatitis Is Essential for Induction of Pancreatic Ductal Adenocarcinoma by K-Ras Oncogenes in Adult Mice. Cancer Cell. 2007; 11:291–302. [PubMed: 17349585]

Guo K, Ma Q, Li J, Wang Z, Shan T, Li W, Xu Q, Xie K. Interaction of the Sympathetic Nerve with Pancreatic Cancer Cells Promotes Perineural Invasion through the Activation of STAT3 Signaling. Molecular Cancer Therapeutics. 2013; 12:264–273. [PubMed: 23288783]

Hassan S, Karpova Y, Baiz D, Yancey D, Pullikuth A, Flores A, Register T, Cline JM, D'Agostino R, Danial N, et al. Behavioral stress accelerates prostate cancer development in mice. J Clin Invest. 2013; 123:874–886. [PubMed: 23348742]

Hayakawa Y, Wang TC. Nerves switch on angiogenic metabolism. Science. 2017; 358:305–306. [PubMed: 29051365]

Hayakawa Y, Sakitani K, Konishi M, Asfaha S, Niikura R, Tomita H, Renz BW, Tailor Y, Macchini M, Middelhoff M, et al. Nerve Growth Factor Promotes Gastric Tumorigenesis through Aberrant Cholinergic Signaling. Cancer Cell. 2017; 31:21–34. [PubMed: 27989802]

Hingorani SR, Petricoin EF, Maitra A, Rajapakse V, King C, Jacobetz MA, Ross S, Conrads TP, Veenstra TD, Hitt BA, et al. Preinvasive and invasive ductal pancreatic cancer and its early detection in the mouse. Cancer Cell. 2003; 4:437–450. [PubMed: 14706336]

Hingorani SR, Wang L, Multani AS, Combs C, Deramaudt TB, Hruban RH, Rustgi AK, Chang S, Tuveson DA. Trp53R172H and KrasG12D cooperate to promote chromosomal instability and widely metastatic pancreatic ductal adenocarcinoma in mice. Cancer Cell. 2005; 7:469–483. [PubMed: 15894267]

Jansen L, Hoffmeister M, Arndt V, Chang-Claude J, Brenner H. Stage-specific associations between beta blocker use and prognosis after colorectal cancer. Cancer. 2014; 120:1178–1186. [PubMed: 24415516]

Kiberstis PA. Cancer and nerves: A tuf(t) partnership. Science. 2017; 355:144–145.

Kim-Fuchs C, Le CP, Pimentel MA, Shackleford D, Ferrari D, Angst E, Hollande F, Sloan EK. Chronic stress accelerates pancreatic cancer growth and invasion: A critical role for beta-adrenergic signaling in the pancreatic microenvironment. 2014:1–8.

Kopp JL, von Figura G, Mayes E, Liu F-F, Dubois CL, Morris JP Iv, Pan FC, Akiyama H, Wright CVE, Jensen K, et al. Identification of Sox9-Dependent Acinar-to-Ductal Reprogramming as the Principal Mechanism for Initiation of Pancreatic Ductal Adenocarcinoma. Cancer Cell. 2012; 22:737–750. [PubMed: 23201164]

Lemeshow S, Sørensen HT, Phillips G, Yang EV, Antonsen S, Riis AH, Lesinski GB, Jackson R, Glaser R. β-Blockers and survival among Danish patients with malignant melanoma: a population-based cohort study. Cancer Epidemiol Biomarkers Prev. 2011; 20:2273–2279. [PubMed: 21933972]

Liebl F, Demir IE, Mayer K, Schuster T, D'Haese JG, Becker K, Langer R, Bergmann F, Wang K, Rosenberg R, et al. The impact of neural invasion severity in gastrointestinal malignancies: a clinicopathological study. Ann Surg. 2014; 260:900–7. discussion907–8. [PubMed: 25379860]

Longair MH, Baker DA, Armstrong JD. Simple Neurite Tracer: open source software for reconstruction, visualization and analysis of neuronal processes. Bioinformatics. 2011; 27:2453–2454. [PubMed: 21727141]

Lorton D, Bellinger DL. Molecular mechanisms underlying β-adrenergic receptor-mediated cross-talk between sympathetic neurons and immune cells. Int J Mol Sci. 2015; 16:5635–5665. [PubMed: 25768345]

Love MI, Huber W, Anders S. Moderated estimation of fold change and dispersion for RNA-seq data with DESeq2. Genome Biol. 2014; 15:550. [PubMed: 25516281]

Madden KS, Szpunar MJ, Brown EB. β-Adrenergic receptors (β-AR) regulate VEGF and IL-6 production by divergent pathways in high β-AR-expressing breast cancer cell lines. Breast Cancer Res Treat. 2011; 130:747–758. [PubMed: 21234673]

Magnon C, Hall SJ, Lin J, Xue X, Gerber L, Freedland SJ, Frenette PS. Autonomic Nerve Development Contributes to Prostate Cancer Progression. Science. 2013; 341:1236361–1236361. [PubMed: 23846904]

Miknyoczki SJ, Lang D, Huang L, Klein-Szanto AJ, Dionne CA, Ruggeri BA. Neurotrophins and Trk receptors in human pancreatic ductal adenocarcinoma: expression patterns and effects on in vitro invasive behavior. Int J Cancer. 1999; 81:417–427. [PubMed: 10209957]

Monje M. Settling a Nervous Stomach: The Neural Regulation of Enteric Cancer. Cancer Cell. 2017; 31:1–2. [PubMed: 28073000]

Myers RB, Oelschlager D, Srivastava S, Grizzle WE. Accumulation of the p53 protein occurs more frequently in metastatic than in localized prostatic adenocarcinomas. Prostate. 1994; 25:243–248. [PubMed: 7971515]

Partecke LI, Speerforck S, Käding A, Seubert F, Kühn S, Lorenz E, Schwandke S, Sendler M, Keßler W, Trung DN, et al. Chronic stress increases experimental pancreatic cancer growth, reduces survival and can be antagonised by beta-adrenergic receptor blockade. Pancreatology. 2016; 16:1–11. [PubMed: 26891820]

Peterson SC, Eberl M, Vagnozzi AN, Belkadi A, Veniaminova NA, Verhaegen ME, Bichakjian CK, Ward NL, Dlugosz AA, Wong SY. Basal Cell Carcinoma Preferentially Arises from Stem Cells within Hair Follicle and Mechanosensory Niches. Cell Stem Cell. 2015; 16:400–412. [PubMed: 25842978]

Pérez Piñero C, Bruzzone A, Sarappa MG, Castillo LF, Lüthy IA. Involvement of α2- and β2-adrenoceptors on breast cancer cell proliferation and tumour growth regulation. Br J Pharmacol. 2012; 166:721–736. [PubMed: 22122228]

R Core Team 2016. R: a Language and Environment for Statistical Computing. 2016. https://www.r-project.org

Rahib L, Smith BD, Aizenberg R, Rosenzweig AB, Fleshman JM, Matrisian LM. Projecting Cancer Incidence and Deaths to 2030: The Unexpected Burden of Thyroid, Liver, and Pancreas Cancers in the United States. Cancer Research. 2014; 74:2913–2921. [PubMed: 24840647]

Reichert M, Takano S, Heeg S, Bakir B, Botta GP, Rustgi AK. Isolation, culture and genetic manipulation of mouse pancreatic ductal cells. Nat Protoc. 2013; 8:1354–1365. [PubMed: 23787893]

Saloman JL, Albers KM, Li D, Hartman DJ, Crawford HC, Muha EA, Rhim AD, Davis BM. Ablation of sensory neurons in a genetic model of pancreatic ductal adenocarcinoma slows initiation and progression of cancer. Pnas. 2016:201512603–201512606.

Schuller HM, Al-Wadei HAN, Ullah MF, Plummer HK III. Regulation of pancreatic cancer by neuropsychological stress responses: a novel target for intervention. Carcinogenesis. 2011; 33:bgr251–196.

Secq V, Leca J, Bressy C, Guillaumond F, Skrobuk P, Nigri J, Lac S, Lavaut MN, Bui TT, Thakur AK, et al. Stromal SLIT2 impacts on pancreatic cancer-associated neural remodeling. Cell Death Dis. 2015; 6:e1592. [PubMed: 25590802]

Sinha S, Fu YY, Grimont A, Ketcham M, Lafaro KJ, Saglimbeni JA, Askan G, Bailey JM, Melchor JP, Zhong Y, et al. PanIN neuroendocrine cells promote tumorigenesis via neuronal crosstalk. Cancer Research. 2017

Stopczynski RE, Normolle D, Hartman DJ, Ying H, Deberry JJ, Bielefeldt K, Rhim AD, Depinho RA, Albers KM, Davis BM. Neuroplastic changes occur early in the development of pancreatic ductaladenocarcinoma. Cancer Research. 2014; 74:1718–1727. [PubMed: 24448244]

Thaker PH, Han LY, Kamat AA, Arevalo JM, Takahashi R, Lu C, Jennings NB, Armaiz-Pena G, Bankson JA, Ravoori M, et al. Chronic stress promotes tumor growth and angiogenesis in a mouse model of ovarian carcinoma. Nature Medicine. 2006; 12:939–944.

Trapnell C, Pachter L, Salzberg SL. TopHat: discovering splice junctions with RNA-Seq. Bioinformatics. 2009; 25:1105–1111. [PubMed: 19289445]

Udumyan R, Montgomery S, Fang F, Almroth H, Valdimarsdottir U, Ekbom A, Smedby KE, Fall K. Beta-blocker drug use and survival among patients with pancreatic adenocarcinoma. Cancer Research. 2017

Watkins JL, Thaker PH, Nick AM, Ramondetta LM, Kumar S, Urbauer DL, Matsuo K, Squires KC, Coleman RL, Lutgendorf SK, et al. Clinical impact of selective and nonselective beta-blockers on survival in patients with ovarian cancer. Cancer. 2015; 121:3444–3451. [PubMed: 26301456]

Weddle DL, Tithoff P, Williams M, Schuller HM. Beta-adrenergic growth regulation of human cancer cell lines derived from pancreatic ductal carcinomas. Carcinogenesis. 2001; 22:473–479. [PubMed: 11238189]

Zahalka AH, Arnal-Estapé A, Maryanovich M, Nakahara F, Cruz CD, Finley LWS, Frenette PS. Adrenergic nerves activate an angio-metabolic switch in prostate cancer. Science. 2017; 358:321–326. [PubMed: 29051371]

Zhang D, Ma QY, Hu HT, Zhang M. β2-adrenergic antagonists suppress pancreatic cancer cell invasion by inhibiting CREB, NFκB and AP-1. Cancer Biol Ther. 2010; 10:19–29. [PubMed: 20424515]

Zhao CM, Hayakawa Y, Kodama Y, Muthupalani S, Westphalen CB, Andersen GT, Flatberg A, Johannessen H, Friedman RA, Renz BW, et al. Denervation suppresses gastric tumorigenesis. Sci Transl Med. 2014; 6:250ra115–250ra115.

Zhu Z, Friess H, diMola FF, Zimmermann A, Graber HU, Korc M, Büchler MW. Nerve growth factor expression correlates with perineural invasion and pain in human pancreatic cancer. J Clin Oncol. 1999; 17:2419–2428. [PubMed: 10561305]

Significance

Stress appears to promote carcinogenesis, but the exact role of the sympathetic nervous (SNS) in pancreatic cancer is unclear. This study investigates the influence of neuropsychological stress and the extensive crosstalk that occurs during pancreatic carcinogenesis between cancer cells and sympathetic nerves. ADRB2 and NGF-BDNF/Trk-pathways are central to pancreatic cancer biology. Targeting these adrenergic and neurotrophin signaling pathways may prove useful in the treatment of PDAC.

Highlights

- Neuropsychological stress accelerates PDAC development via ADRB2-signaling
- ADRB2-signaling upregulates NGF and BDNF, thereby increasing nerve density
- Blockade of the ADRB2 and NGF/Trk pathway prolongs survival in KPC mice
- ADRB2 and NGF-BDNF/Trk-pathways may be promising targets in PDAC treatment

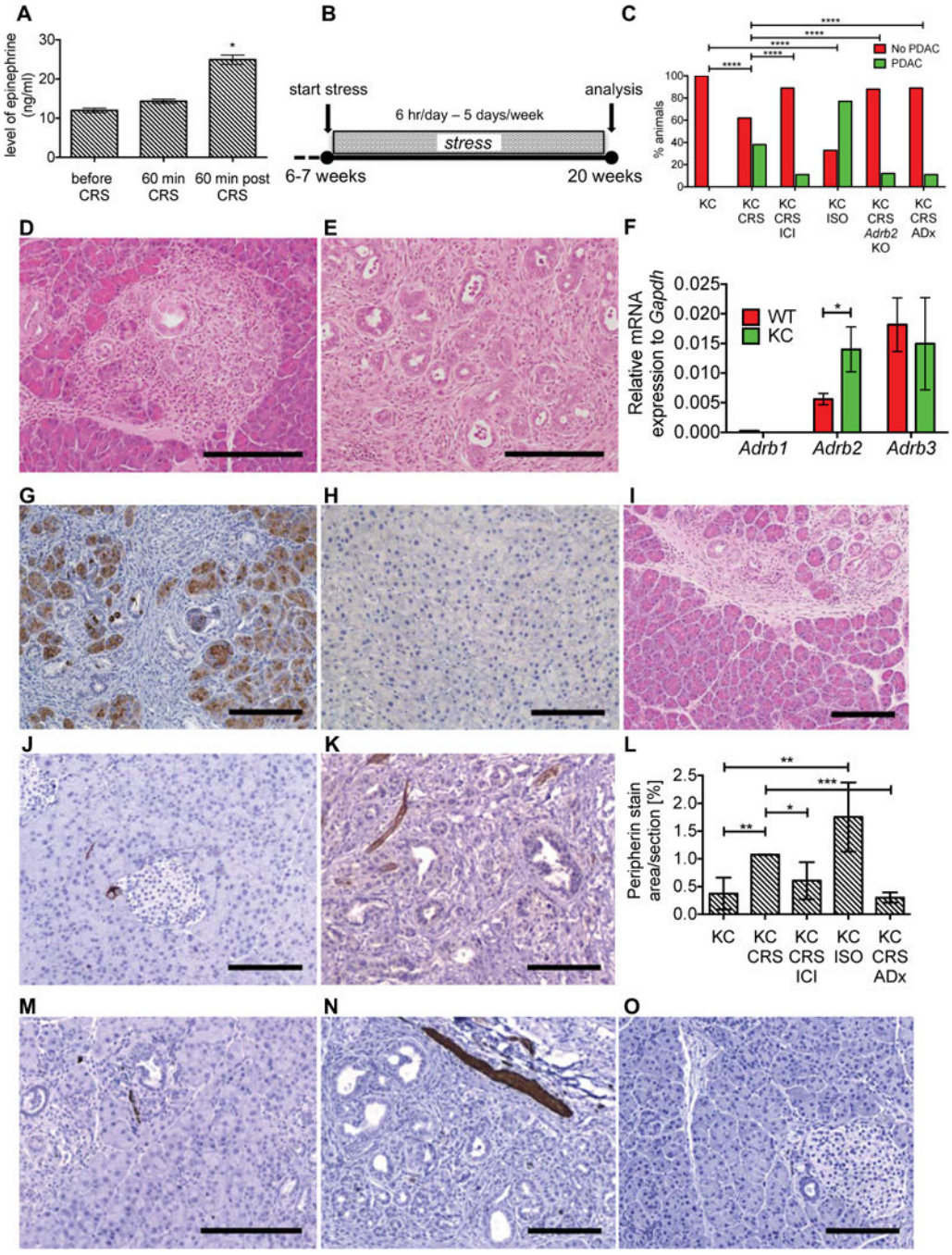

Figure 1. Chronic Neuropsychological Stress Promotes *Kras* Induced Pancreatic Carcinogenesis

(A) Systemic epinephrine levels in KC mice measured by ELISA before, 60 min in stress and 60 min after stress.

(B) Experimental set up: mice were stressed starting at 6 weeks of age for 6 hr/day, 5 days/week until 20 weeks of age.

(C) Incidence of PDAC at 20 weeks of age in control KC mice (KC) (n=12), stressed KC mice (KC CRS) (n=13), stressed KC mice treated with ICI 118,551 (ICI) before stress was applied (KC CRS ICI) (n=12), KC mice treated with isoproterenol (ISO) continuously from

6-7 weeks to 20 weeks (KC ISO) (n=12), stressed KC-*Adrb2* KO mice (KC CRS *Adrb2* KO) (n=8), and stressed KC mice after bilateral adrenalectomy at 6-7 weeks of age (KC CRS ADx) (n=12).

(D, E) Representative images of pancreatic H&E slides from KC **(D)** and KC CRS mice **(E)** at 20 weeks.

(F) Relative quantification of *Adrb1*, *Adrb2*, and *Adrb3* mRNA expression in pancreata from WT mice and KC mice (n=3, respectively).

(G, H) Representative images of immunohistochemistry (IHC) for ADRB2 in pancreata from KC **(G)** and WT mice **(H)**.

(I) Representative image of a pancreatic H&E slide from KC CRS ICI mice at 20 weeks.

(J, K) Representative images of IHC for peripherin in pancreata from KC **(J)** and KC CRS mice **(K)**.

(L) Quantification of the peripherin^{+} area in pancreata from KC (n=12), KC CRS (n=13), KC CRS ICI (n=12), KC ISO (n=12), and KC CRS ADx (n=12) at 20 weeks.

(M-O) Representative images of IHC for peripherin in pancreata from KC CRS ICI **(M)**, KC ISO **(N)**, and KC CRS ADx mice **(O).**

Scale bars, 200 μm. Means ± SEM. *p<0.05; **p<0.001; ***p<0.0001. See also Figure S1.

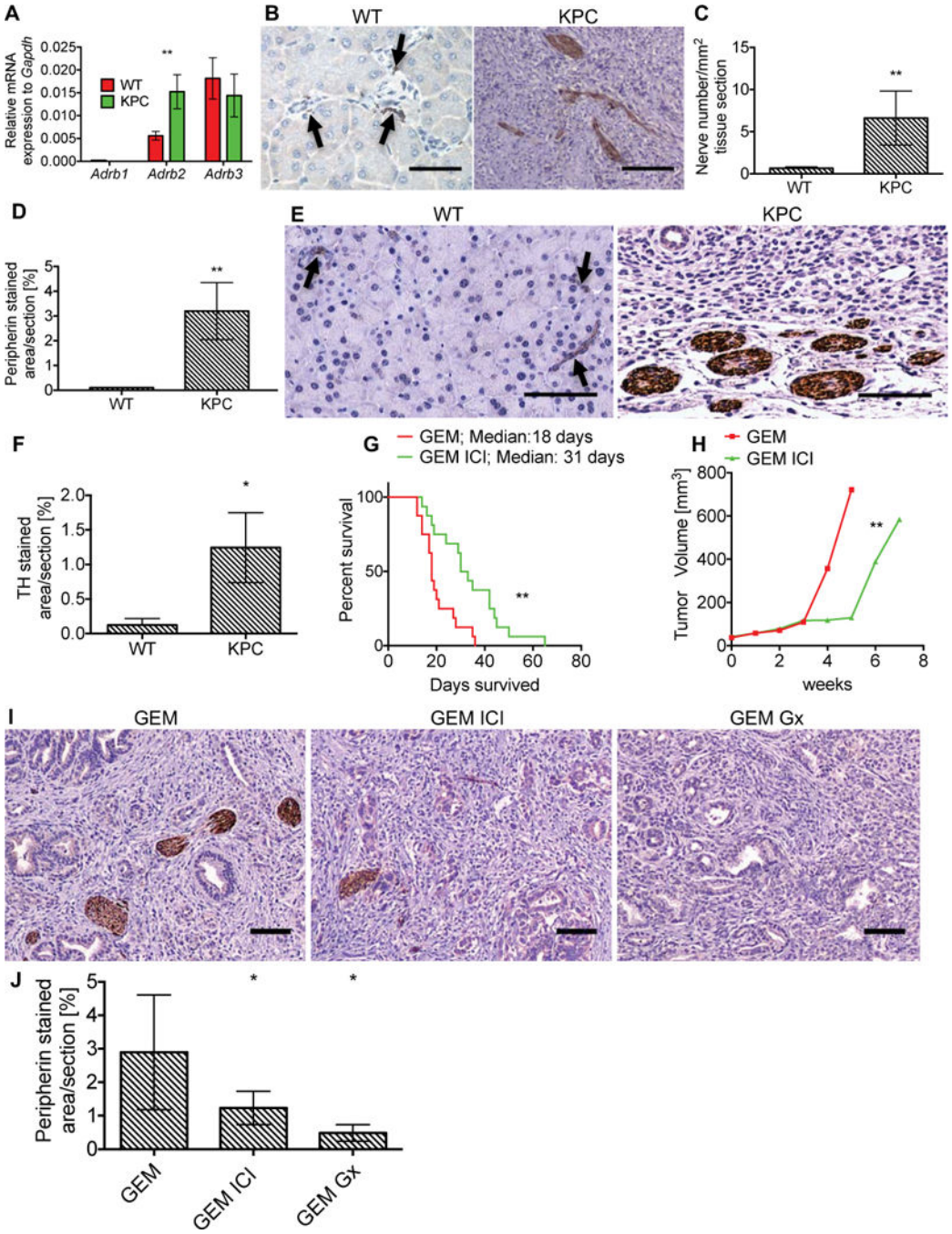

Figure 2. ADRB2 Blockade Significantly Increases Overall Survival in KPC Mice

(A) Relative quantification of *Adrb1, Adrb2*, and *Adrb3* mRNA expression in pancreata from WT mice and PDAC from KPC mice. **p<0.001.

(B) Representative photographs of peripherin IHC in the pancreas of WT mice and PDAC of KPC mice. Black arrows indicate small nerves in normal pancreatic tissue.

(C, D) Bar graphs showing quantification of peripherin staining in pancreata from WT and PDAC from KPC mice (n=15 each group) as neural density (nerve number/mm^2 tissue

section) (**p=0.0093) **(C)** and positively stained neuronal area (peripherin stained area/ section [%]) (**p=0.0087) **(D)**.

(E) Representative photographs of tyrosine hydroxylase (TH) IHC in the pancreas from WT mice and PDAC from KPC mice. Black arrows indicate small TH^+ nerves in normal pancreatic tissue.

(F) Bar graph showing quantification of TH^+ staining in pancreata from WT mice and PDAC from KPC mice (TH stained area/section [%]). *p=0.0061.

(G) Kaplan-Meier curves of KPC mice treated with gemcitabine (GEM; n=16) and KPC mice treated with gemcitabine and ICI 118,551 (GEM ICI; n=16) enrolled with tumors of 20-60 mm^3. **p=0.0038. This experiment and Figure S2H were conducted at the same time and have the same control group.

(H) Tumor volume curves of KPC mice treated as shown in **(G)**. (GEM; n=16, GEM ICI n=16). **p=0.0026.

(I) Representative images of peripherin IHC in PDAC from KPC mice treated with gemcitabine (GEM), gemcitabine and ICI 118,551 (GEM ICI), and gemcitabine and ganglionectomy (GEM Gx).

(J) Bar graph showing quantification of the area stained positive for peripherin in PDAC from KPC mice treated with GEM, GEM ICI, and GEM Gx. *p<0.05.

Means ± SEM. Scale Bars, 200 μm. See also Figure S2.

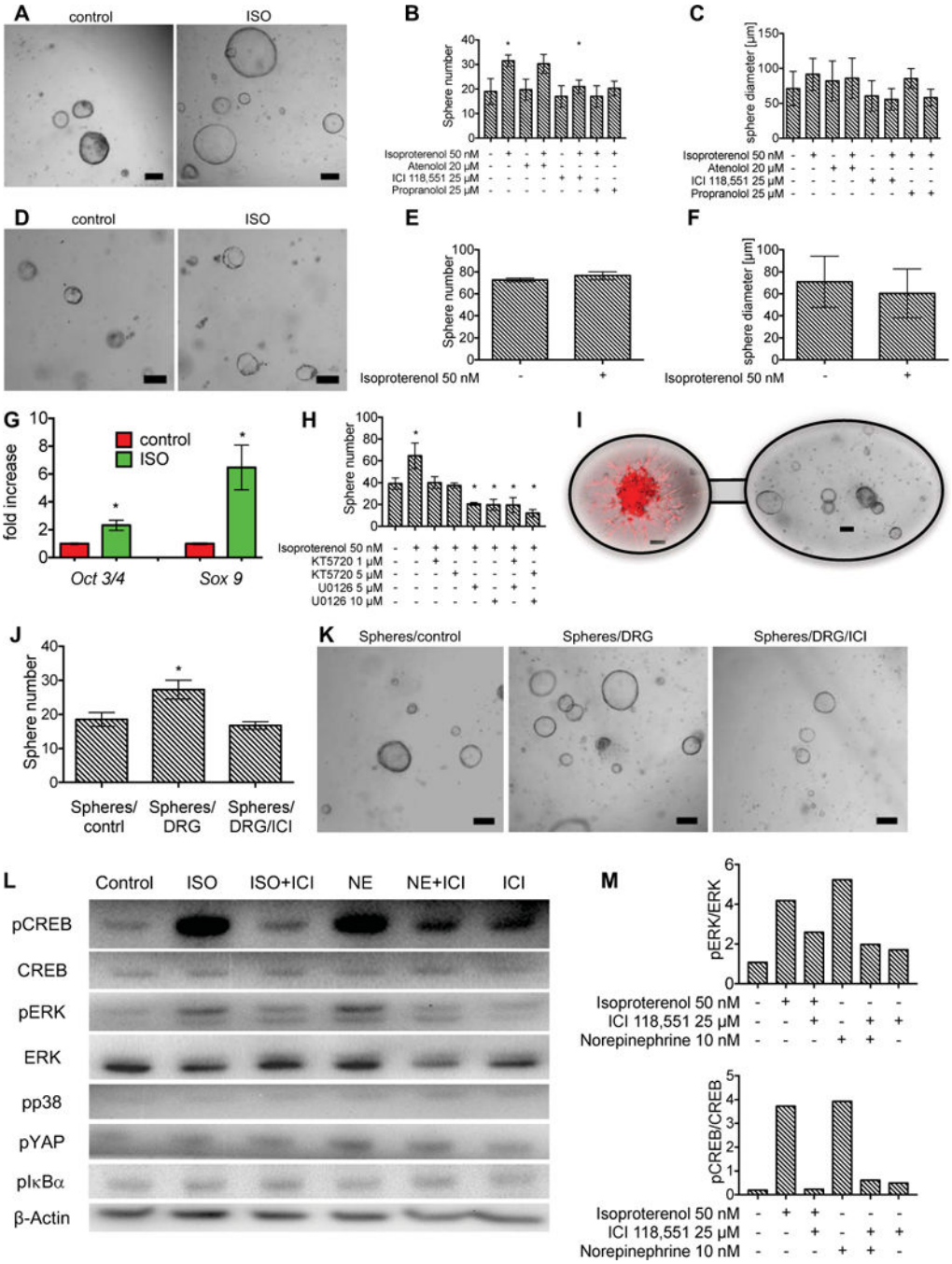

Figure 3. Catecholamines Promote Acinar to Ductal Metaplasia and Drive Proliferation

(A) Representative photographs of 3D pancreatic spheres isolated from LSL-*Kras*$^{+/G12D}$ mice treated with an Adeno-Cre virus alone (control) or together with ISO (ISO).

(B, C) Quantification of number **(B)** and size **(C)** of LSL-*Kras*$^{+/G12D}$ pancreatic spheres treated with an Adeno-Cre virus and the substance indicated after 7 days in culture.

(D) Representative photographs of 3D pancreatic spheres from LSL-*Kras*$^{+/G12D}$;*Adrb2* KO mice treated with an Adeno-Cre virus alone (control) or together with ISO (ISO).

(E, F) Quantification of number **(G)** and size **(H)** of LSL-*Kras*$^{+/G12D}$;*Adrb2* KO pancreatic spheres treated with an Adeno-Cre virus and ISO after 7 days in culture.
(G) Fold increase in mRNA expression of *Oct3/4* and *Sox9* in LSL-*Kras*$^{+/G12D}$ pancreatic spheres treated with an Adeno-Cre virus alone (control) or together with ISO (ISO).
(H) Quantification of number of LSL-*Kras*$^{+/G12D}$ pancreatic spheres treated with an Adeno-Cre virus and ISO, KT5720 and U0126; after 7 days in culture.
(I) Experimental set up of co-culture studies using pancreatic spheres from LSL-*Kras*$^{+/G12D}$;*Pdx1*-Cre mice (KC) (right) and DRGs (red) from E14.5 old mTmG murine embryos in a separate Matrigel dot (left), spheres and DRG dots are connected via a Matrigel bridge.
(J) Quantification of number of pancreatic spheres isolated from KC mice and placed next to a Matrigel dot (spheres/control), a Matrigel dot containing a DRG from an E14.5 old mTmG murine embryo (spheres/DRG) and a Matrigel dot containing a DRG from an E14.5 old mTmG murine embryo and treated with ICI (spheres/DRG/ICI).
(K) Representative photographs of 3D pancreatic spheres, cocultured as described in **(J)**.
(L) Western Blot analyzing signaling pathways after ISO or norepinephrine (NE) and/or ICI treatment in Panc-1 cells.
(M) Quantification of densitometry of Western Blot depicted in **(L)** for phosphorylated ERK (pERK)/ERK and phosphorylated CREB (pCREB)/CREB.
Means ± SEM. *p<0.05. Scale Bars, 100 μm. See also Figure S3.

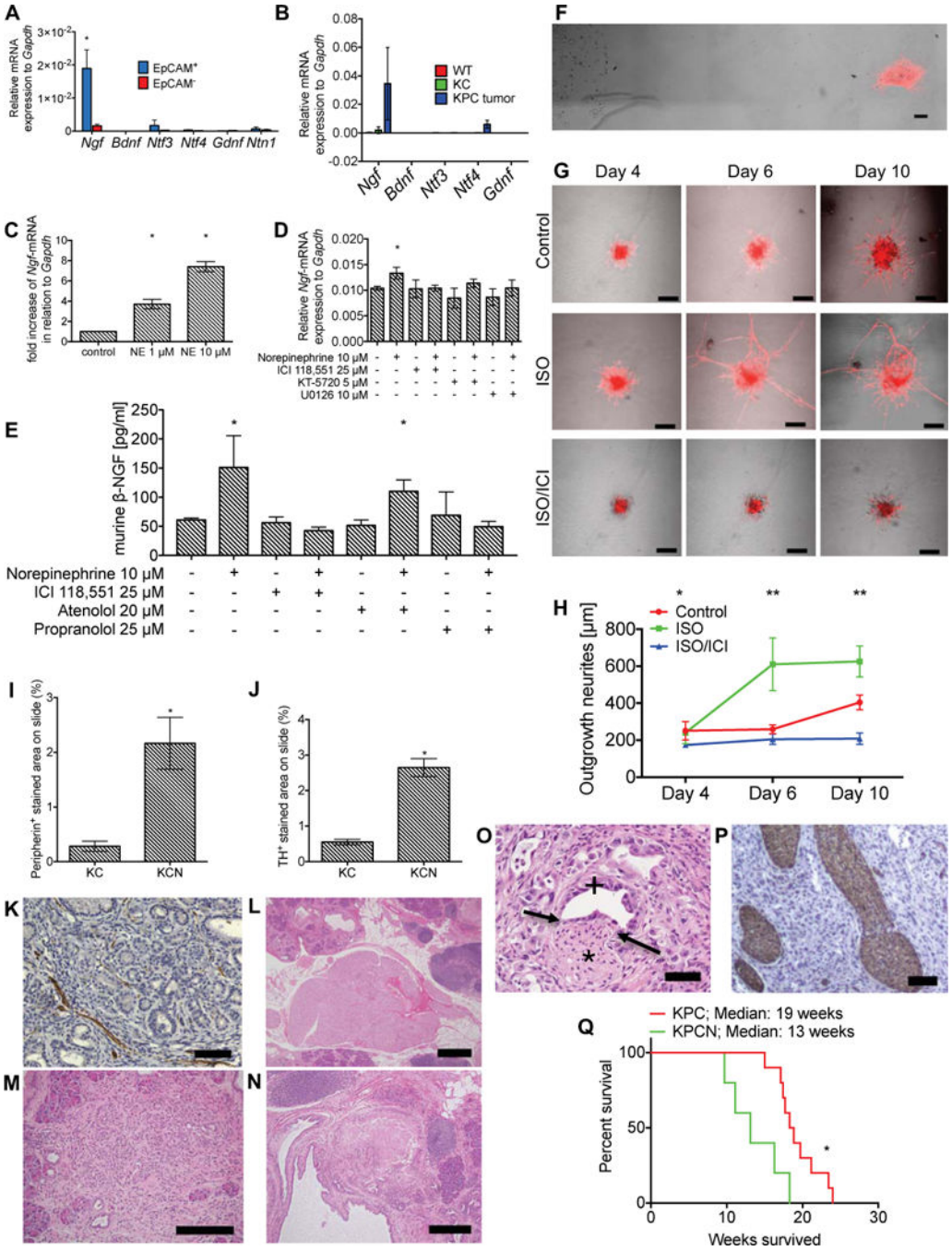

Figure 4. Adrenergic Signaling Increases Neurotrophin Secretion and Promotes PDAC Development through Tumor-Associated Axonogenesis

(A) Relative quantification of mRNA expression of neurotrophins and axonal guidance proteins in KPC tumors sorted for $EpCAM^+$ and $EpCAM^-$ cells (n=6).

(B) Relative quantification of mRNA expression of NTs in pancreata from WT, KC mice and PDAC from KPC mice (n=5 per group).

(C) Relative quantification of mRNA expression of *Ngf* in K8282 cells after stimulation with increasing concentrations of NE.

(D) Relative quantification of mRNA expression of *Ngf* in K8282 cells after stimulation with NE and pretreatment with ICI, KT5720 and U0126.
(E) Murine β-NGF levels measured by ELISA in the supernatant of K8282 cells after stimulation with NE and pretreatment with ICI, atenolol, and propranolol.
(F) Experimental set up of co-culture studies using K8282 cells (left side) and DRGs from E14.5 old mTmG murine embryo (red, right side). Scale bar, 200 μm.
(G) Representative confocal pictures of DRGs from E14.5 mTmG murine embyos cultured next to K8282 cells as depicted in **(F)**, control, treated with ISO (ISO), and pretreated with ICI before ISO treatment (ISO/ICI) after 4, 6 and 10 days in co-culture, respectively. Scale bars, 200 μm.
(H) Quantification of axonogenesis from DRGs in co-culture with K8282, without treatment (control), treated with ISO, and pretreated with ICI before ISO treatment (ISO/ICI) at 4, 6 and 10 days in co-culture.
(I) Quantification of the peripherin^{+} stained area (IHC) in pancreata from KC and KCN mice (n=5) at 20 weeks.
(J) Quantification of the TH^{+} stained area (IHC) in pancreata from KC and KCN mice (n=5).
(K) Representative image of pancreatic peripherin IHC in 20-week-old KCN mice. Scale bar, 200 μm.
(L-N) Representative images of pancreatic sections (H&E) from KCN mice at 20 weeks showing an enlarged intrapancreatic ganglion **(L)**, foci of micronodular small duct **(M)** and large duct **(N)** intraepithelial neoplasia (PanIN-3). Scale bars, 100 μm in **(M)**, 200 μm in **(L)** and **(N)**.
(O) Representative image of H&E staining showing perineural invasion (arrows) in a pancreatic section from a KPCN mouse. Black star indicates a intratumoral nerve. Cross indicates tumor cells. Scale bar, 50 μm.
(P) Representative image of pancreatic peripherin IHC in KPCN mice. Scale bar, 200 μm.
(Q) Kaplan-Meier curves showing OS of KPC (n=12) and KPCN (n=6) mice.
Means ± SEM. *p<0.05, **p<0.005. See also Figure S4.

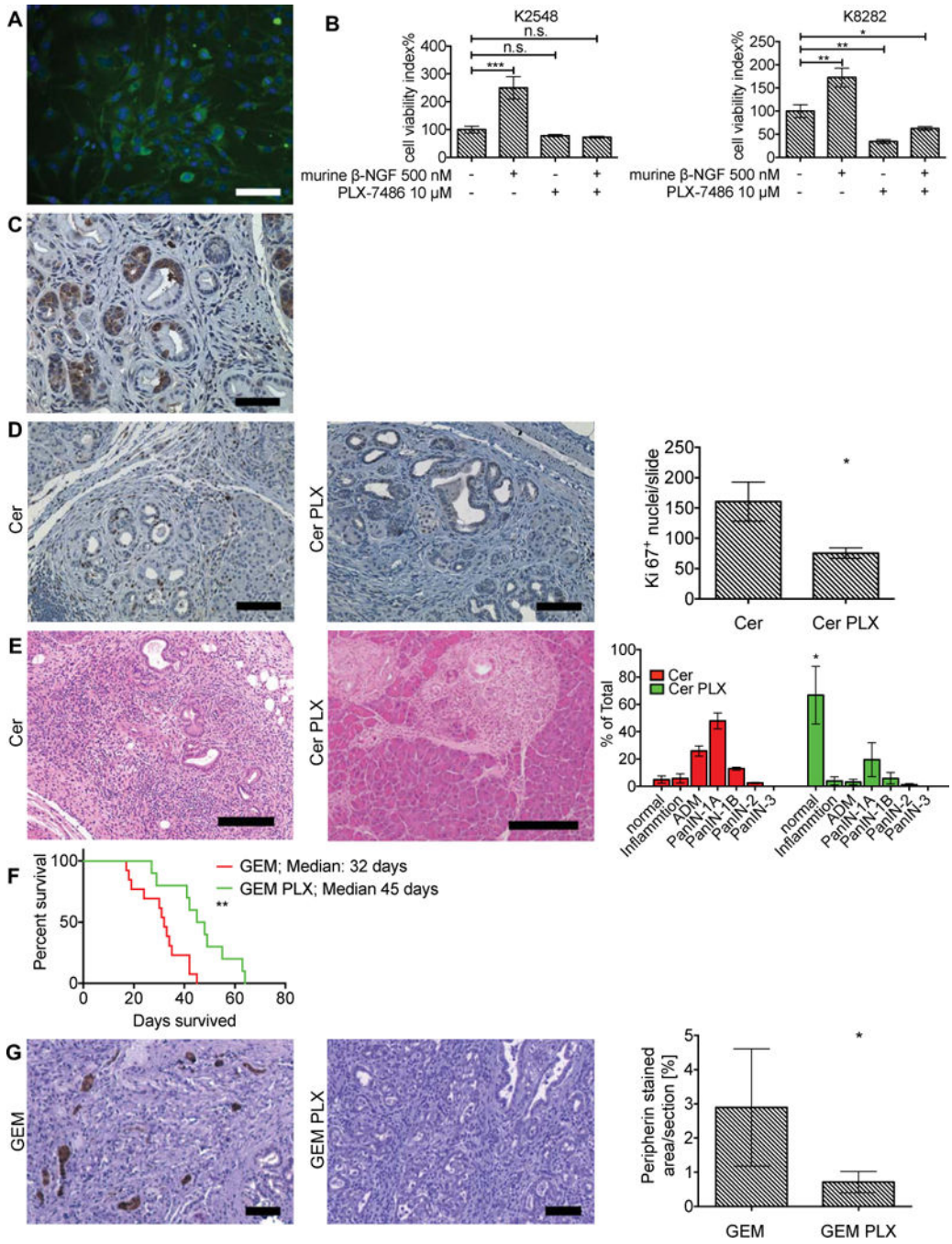

Figure 5. Blockade of NGF/Trk Pathway Inhibits Proliferation and Innervation and Increases Overall Survival in KPC Mice

(A) Representative image of pan-Trk immunocytochemistry (ICC) of K8282 cells.

(B) MTT-assay of murine PDAC cells K2548 and K8282 treated with murine β-NGF with and without pretreatment of PLX-7486.

(C) Representative image of pancreatic pan-Trk IHC of cerulein-injected KC mice at 20 weeks.

(D) Representative image of pancreatic Ki67 IHC of cerulein-injected KC mice at 20 weeks on control diet (Cer) and PLX-7486 containing diet (Cer PLX); Quantification of Ki67 staining of pancreata depicted (n=10 mice per group) (right).
(E) Representative image of pancreatic H&E staining of cerulein-injected KC mice at 20 weeks on control diet (Cer) and PLX-7486 containing diet (Cer PLX); Pathological scoring of PanINs of pancreata depicted (n=10 mice each group).
(F) Kaplan-Meier curves of KPC mice enrolled with tumor diameters of 3-6 mm and treated by GEM biweekly on control diet (GEM) (n=13) or by GEM biweekly on PLX-7486 containing diet (GEM PLX) (n=10).
(G) Representative images of peripherin IHC in PDAC from KPC mice treated with GEM (GEM) and KPC mice treated with GEM and PLX-7486 (GEM PLX); Bar graph showing quantification of peripherin staining of pancreata depicted (GEM n=10 and GEM PLX n=13 mice).
Means ± SEM. *p<0.05, **p<0.005; ***p<0.001. Scale bars, 200 μm. See also Figure S5.

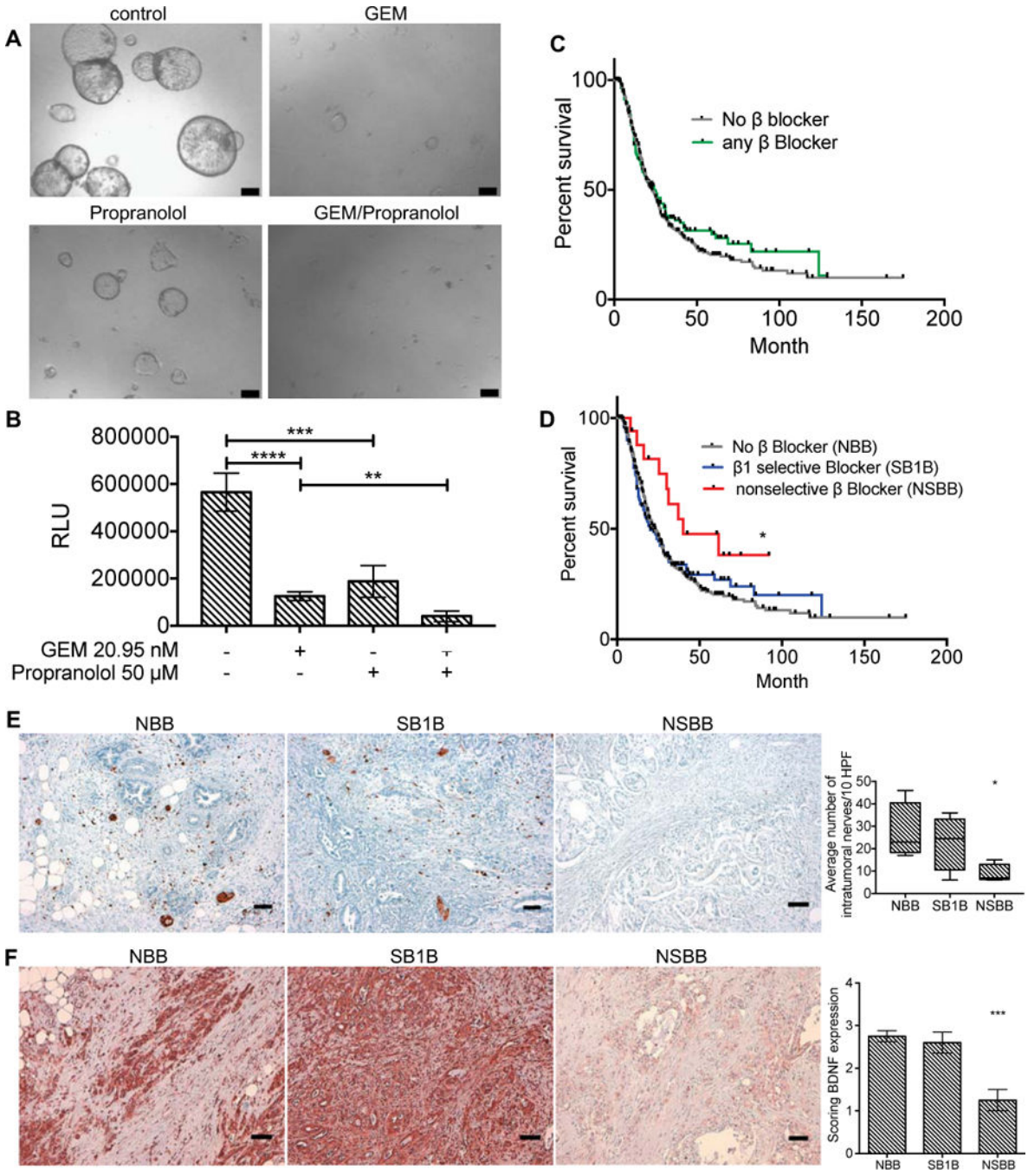

Figure 6. Nonselective β-Blocker Treatment Increases Overall Survival in Surgically Resected PDAC Patients

(A) Representative photographs of organoids generated from primary resected human PDAC specimen, control, GEM treated, propranolol (Propranolol) treated and propranolol and GEM treated (GEM/Propranolol) cultures.

(B) Bar graph shows quantification of relative light units (RLU) of treated human PDAC organoid cultures (**p=0.0071; ***p<0.0001; ****p=0.0002).

(C) Kaplan-Meier curves of PDAC patients (n=631) comparing patients without β-blocker medication (grey line) (n=427) and any β-blocker (green line) (n=168) after surgical resection of the primary tumor.
(D) Kaplan-Meier curves of PDAC patients (n=631) comparing patients without β-blocker medication (grey line) (n=427), β1-selective agents (blue line) (n=151) and nonselective β-blockers (red line) (n=17) after surgical resection of the primary tumor, *p=0.031.
(E) Representative images of IHC for protein S-100 from PDAC sections from patients having no β-blocker (NBB, n=8), β1-selective agents (SB1B, n=8) and a nonselective β-blocker (NSBB, n=5) (3 sections/patient; Bar graph shows average number of intratumoral nerves/10 high power fields (HPF) (3 sections/patient, *p=0.0338).
(F) Representative images of IHC for BDNF from tumor sections from NBB (n=8), SB1B (n=8) and NSBB patients (n=5) (3 sections/patient); Bar Graph showing average scoring of BDNF IHC (3 sections/patient, ***p<0.0001) (right).
Means ± SEM. Scale Bars, 50 μm in **(A)**, 100 μm **(E)** and **(F).** See also Figure S6.